GENOME-WIDE *IN VIVO* CRISPR ACTIVATION SCREEN TO IDENTIFY

GENETIC DRIVERS OF NON-SMALL CELL LUNG CANCER BRAIN

METASTASIS

GENOME-WIDE *IN VIVO* CRISPR ACTIVATION SCREEN TO IDENTIFY GENETIC

DRIVERS OF NON-SMALL CELL LUNG CANCER BRAIN METASTASIS

By NIKOO AGHAEI, HON. B.SC.

A Thesis Submitted to the School of Graduate Studies in Partial Fulfilment of the Requirements for the Degree Master of Science

DESCRIPTIVE NOTE

MASTER OF SCIENCE (2021)

Biochemistry & Biomedical Sciences McMaster University
Hamilton, Ontario

TITLE: Genome-wide *in vivo* CRISPR activation screen to identify genetic drivers of non-small cell lung cancer brain metastasis

AUTHOR: Nikoo Aghaei, Hon. B.Sc. (McMaster University)
SUPERVISOR: Dr. Sheila Kumari Singh
NUMBER OF PAGES: 89

LAY ABSTRACT

Brain metastasis, or the spread of a primary cancer from another organ to the brain, is the most common adult brain tumor. Brain metastases can arise after the treatment of primary tumors and are only detected in the clinic at a highly malignant stage. Current treatments for brain metastasis consist of surgical removal and palliative chemoradiotherapy, which fail to fully eliminate the brain tumor. Over 20% of cancer patients develop brain metastases, with lung, breast, and skin cancers leading as the top three sources of metastasis. In particular, 40% of patients with non-small cell lung cancer develop brain metastasis, with survival of only 4-11 weeks once diagnosed without treatment, and 16 months with treatment. As systemic therapies for the treatment of non-small cell lung cancer are becoming increasingly effective at controlling primary disease, patients are ironically succumbing to their brain tumors. This highlights a large unmet need to develop novel targeted therapies for the treatment of lung-to-brain metastases (LBM). Functional genomic tools provide the opportunity to investigate the genetic underpinnings of LBM. With the advent of gene editing technologies, we are able to overexpress various genes and observe the impact genetic perturbations have on tumor initiation, growth, and metastasis.

In this thesis, we devised a pre-clinical animal model of LBM that could be used to study genetic drivers of LBM using a gene overexpression tool such that one gene per tumor cell gets activated. We are then able to model the disease trajectory from a lung tumor to brain metastasis development using patient samples in our animal model and identify genes that, upon overexpression, drive LBM. This platform will lead to potential therapeutic targets to

prevent the formation of LBM and prolong the survival of patients with non-small cell lung cancer.

ABSTRACT

Brain metastasis (BM), the most common tumor of the central nervous system, occurs in 20-36% of primary cancers. In particular, 20-40% of patients with non-small cell lung cancer (NSCLC) develop brain metastases, with a dismal survival of approximately 4-11 weeks without treatment, and 16 months with treatment. This highlights a large unmet need to develop novel targeted therapies for the treatment of lung-to-brain metastases (LBM). Genomic interrogation of LBM using CRISPR technology can inform preventative therapies targeting genetic vulnerabilities in both primary and metastatic tumors. Loss-of-function studies present limitations in metastasis research, as knocking out genes essential for survival in the primary tumor cells can thwart the metastatic cascade prematurely. However, transcriptional overexpression of genes using CRISPR activation (CRISPRa) has the potential for overcoming dependencies of gene essentiality.

In this thesis, we created and utilized an *in vivo* genome-wide CRISPRa screening platform to identify novel genes, that when overexpressed, drive LBM. We have developed a patient-derived orthotopic murine xenograft model of LBM using a patient-derived NSCLC cell line (termed CRUK cells) from the Swanton Lab TRACERx study. We introduced a human genome-wide CRISPRa single guide RNA (sgRNA) library into non-metastatic and pro-metastatic lung cancer CRUK cells to achieve 500X representation of each sgRNA in the activation library. We then injected the cells into the lungs of immunocompromised mice and tracked lung tumor development and BM formation. Upon sequencing primary lung tumors and subsequent BM, we will identify enriched sgRNAs which may represent novel drivers of primary lung tumor formation and LBM.

To the best of our knowledge, this study is the first *in vivo* genome-wide CRISPR activation screen using patient-derived NSCLC cells to help elucidate drivers of LBM. This work serves to provide a framework to gain a deeper understanding of the regulators of BM formation which will hopefully lead to targeted drug discovery that will ultimately be used in clinical trials to help eradicate brain metastasis in NSCLC patients.

ACKNOWLEDGEMENTS

I am grateful today to have had the opportunity to work not only on an important project that is near to my heart, but also have had the privilege of meeting such a special group of people throughout my time in the Singh Lab. Having started my time here almost three years ago, I had never imagined how much scientific, academic, and personal growth I would experience through working with influential mentors such as Dr. Sheila Singh. Dr. Singh, I am forever grateful to you for giving me the opportunity to be your student, and for always believing in me even when experiments wouldn't go as planned. I felt supported by you not only in a research capacity, but also in finding my career directions and aspirations.

I was fortunate enough to have the mentorship of Dr. Chitra Venugopal, who has always been there, rain or shine, for all of us in the Singh Lab. Chitra, you have put a new meaning to the word mentor for me. The way you make us feel seen and safe and supported is something that I am most grateful for. You are truly a star in the lab, and we cannot thank you enough for that. I want to also thank my first ever mentor in the Singh Lab that is so special to me, Dr. Blessing Bassey-Archibong. Blessing, you are truly a "blessing" in my life! I remember our times together in TC, learning so much from you, and finding joy in everyday work when you were there. You have truly shaped the way I conduct science and I am forever grateful for the gift of mentorship and most importantly friendship that you have given me. I am also in awe of you and your strength through everything you have achieved during the time I have known you, and it inspires me every day. Next, I want to especially thank my dear mentor Dr. Fred Lam, who has been there for me at every step of the way these past two years and taught me so so much about not only brain metastasis research but also life in general. Fred, I am eternally grateful for the incredible example of a clinician-scientist you have set for me, and I cannot thank you enough for the encouragement and honest feedback you always were so generous to provide for me. From you, I have learned to always persevere, to innovate, and to have the courage to improvise. Brain mets team is so fortunate to have you, and we miss you every day!

To my committee members, Dr. Gurmit Singh, Dr. Yu Lu, and Dr. Jason Moffat, and my mentor Dr. Ekkehard Kasper, I am incredibly grateful for your guidance and insights that have shaped this thesis and my scientific perspectives. Dr. Moffat, I am so appreciative of the support you and your past and present lab members, including Katie Chan, Kevin Brown, Amy Tong, Patricia Mero, Andrea Habsid and David Tieu. You all have generously helped me with this project, and I am so grateful for your knowledge and guidance. I would like to thank Dr. Charles Swanton and Dr. Rob Hynds from Francis Crick Institute for providing us with the opportunity to conduct this research and for their time and guidance throughout these past years. I would like to thank all the funding agencies that have enabled this work, and especially the Brain Tumor Foundation of Canada for their constant support and for giving me the opportunity to present at the undergraduate research symposium. I would also like to thank the Broad Institute, specifically Briana Fritchman, for providing us with guide RNAs.

Next, I would like to thank the Brain metastasis team: how is it possible that so many awesome human beings gather in one place, one team, and work so well together? Agata, I want to thank you for being not only an incredible scientist to look up to, but also an amazing friend that I knew I could always count on. It has been such a privilege for me to witness your work in the lab, and it motivated me to pursue a graduate degree myself. I cannot wait to see what the future holds for you, and I am so happy to have been on the same team as you! Arun, I will never forget the support you provided me with these past few months with the screens, especially those sessions in IVIS. I am so grateful for your help and your playlist choices. Daniel, although I have known you for a few months, I am so thankful for your interest in the projects within the brain mets group and for your help with everything so far! You are an inspiration to all of us.

To everyone at Singh lab, Team MB, Team GBM, Minomi, past Singh lab members, our amazing collaborators, and everyone who I have crossed paths with, thank you for everything you have done for me and for the amazing times that we have had together. Your support means the world to me, and I am inspired by each and every one of you.

Our work would not be what it is today without the generosity of our patient donors. One of the reasons I gravitated towards the Singh lab in the first place was the direct contact with patients. Thinking about how fortunate we are to be able to connect with patients going through some of the hardest times in their lives, it has motivated me more and more to continue the work in the lab.

I want to thank my incredible friends and family for the unconditional love and support throughout my undergraduate and graduate degree. Maman and Baba, your constant support and encouragement was such a strong driving force in my work. Novin, I learned from you to find the fun in everything, and I carried that with me into my everyday work. You all are the center of my world, and I am forever grateful to you all for believing in me. To my friends, I appreciate you all amazing human beings so much. and thank you for listening to me talk about my research.

I dedicate this thesis to all the patients who have been so kind and generous to enable this research, to my amazing family and friends, to all of my mentors, and to the fabulous Singh lab family.

TABLE OF CONTENTS

LIST OF FIGURES

CHAPTER 1 FIGURES

CHAPTER 2 FIGURES

CHAPTER 3 FIGURES

LIST OF SYMBOLS AND ABBREVIATIONS

AKT2	AKT Serine/Threonine Kinase 2
ALK	Anaplastic Lymphoma Kinase
BM	Brain Metastasis
CCNE1	Cyclin E1
CD4	Cluster of differentiation 4
CD45	Cluster of differentiation 45
CDK6	Cyclin dependent Kinase 6
CRISPR-Cas9	Clustered Regularly Interspaced Short Palindromic Repeats-CRISPR associated protein 9
CRISPRa	CRISPR Activation
CRISPRi	CRISPR Interference
dCas9	Dead CRISPR associated protein 9
dCas9-VP64	Dead CRISPR associated protein 9-Viral Protein 64
dsDNA	Double stranded DNA
EGFR	Epidermal Growth Factor Receptor
ERBB2	Erb-B2 Receptor Tyrosine Kinase 2
gDNA	Genomic DNA
GFP-Luc	Green Fluorescent Protein-Luciferase
IVIS	In Vivo Imaging System
KRAS	Kirsten Rat Sarcoma viral oncogene homolog
LBM	Lung-to-Brain Metastasis
MCL1	Myeloid Cell Leukemia-1
MET	MET proto-oncogene
MMP13	Matrix Metallopeptidase 13
MYC	MYC Proto-Oncogene
NGS	Next Generation Sequencing
NSCLC	Non-Small Cell Lung Cancer
NSCLC-BM	Non-Small Cell Lung Cancer Brain Metastasis
NSG	NOD Scid Gamma
PBS	Phosphate Buffered Saline
PDX	Patient-Derived Xenograft
sgRNA	Single Guide RNA
TP53	Tumor Protein 53
TRACERx	TRAcking Cancer Evolution through therapy/Rx
VEGF	Vascular Endothelial Growth Factor A
YAP1	Yes-Associated Protein 1

DECLARATION OF ACADEMIC ACHIEVEMENT

During my graduate studies, I contributed to four projects within Singh lab, two of which are manuscripts currently in preparation and under review, and one review paper (in preparation). I presented at six local and international conferences and was awarded distinctions. In this thesis, I contributed to experimental design, execution, data collection, data analysis and interpretation, and writing of all sections. The work described in this thesis is a result of the combined effort of myself, Dr. Fred Lam, Dr. Chitra Venugopal, Dr. Blessing Bassey-Archibong, Agata Kieliszek, Arun Parmar, and Chirayu Chokshi, under the supervision of Dr. Sheila K. Singh. It was built from the pre-clinical mouse model of lung-to-brain metastasis developed by Dr. Mohini Singh established in her doctoral studies in the Singh lab. Dr. Sheila K. Singh supervised all research projects and aided in experiment design ideation, data interpretation, alongside Dr. Chitra Venugopal and Dr. Fred Lam. Patient-derived non-small cell lung cancer xenograft samples were provided by Dr. Charles Swanton and Dr. Rob Hynds thought the TRACERx study, and cell lines were developed with the help of Dr. Blessing Bassey-Archibong and Dr. Fred Lam. Guidance regarding CRISPR library amplification, sequencing, and CRISPR study design was provided by members of Dr. Jason Moffat's team, including Katherine Chan, Kevin Brown, Amy Tong, David Tieu, and Andrea Habsid.

CHAPTER 1: Introduction

1.1 The Clinical and Molecular Landscape of Brain Metastasis

Brain metastasis (BM) is the most common tumor of the central nervous system, presenting ten times more frequently than primary brain tumors in the clinic (Palmieri, 2012). As systemic therapies for primary cancers improve, circulating tumor cells are allowed more time to metastasize and seed other organs. Commonly used BM therapies include stereotactic radiosurgery, chemoradiotherapy, and whole brain radiation therapy (Lin & DeAngelis, 2015). While these can shrink individual or multiple BM nodules, they are not curative as BM can lay dormant or spread to untreated brain areas (Patchell, 2003). Evaluation of the genetic factors that drive BM will inform predictive biomarkers and future targeted therapies against BM. *In vivo* functional genomics enable the study of interactions between tumor cells and the brain microenvironment and can serve as a robust tool to uncover metastatic driver genes and test therapeutic agents against metastasis.

1.1.1 Epidemiology

It is estimated that between 20-36% of patients with systemic cancers will develop BM at some point in their lives (Villano et al., 2015). The three most common primary cancers to metastasize to the brain are lung (20-56%), breast (5-20%), and melanoma (7-16%) (Barnholtz-Sloan et al., 2004; Berghoff et al., 2016; Nayak, Lee, & Wen, 2012; Sperduto et al., 2010). Lung cancer spreads to the brain irrespective of patient sex and is the most common cause of BM in men. As indicated in a retrospective cohort study from the Nationwide Inpatient Sample, which is the largest database of inpatient admissions in the United States, there has been a 79% relative increase in the annual incidence of BM surgical

resection, from 3900 in 1988 to 7000 in 2000 (Barker, 2004). The increasing prevalence of BM can be attributed to improvements in diagnostic imaging techniques and/or well-controlled primary cancers that extend patients' survival and allow more time for BM development.

1.1.2 The Brain Metastatic Cascade

It is known that cancer cells from specific subclones of the primary tumor break away and invade the surrounding tissue, venules, capillaries, and the lymphatic system **(Figure 1)**. During this process of intravasation, tumor cells interact with immune cells such as macrophages and develop actin-rich degradative protrusions, which promote tumor cell motility *via* clearance of extracellular matrix (Berghoff & Preusser, 2015).

After entering the circulation, tumor cells await an opportunity to undergo metastatic extravasation into the same or a different organ, facilitated by adhesive (circulatory) arrest. The microcapillary network of the brain is dense, and along with a high proportional blood flow, the brain provides a prime opportunity for circulating tumor cells to arrest in movement. Once arrested, tumor cells are required to overcome the blood-brain barrier, which is a highly selective semipermeable border that separates the circulating blood from the central nervous system, and is composed of specialized endothelial cells with low transcytosis rates and a high density of efflux pumps that are connected by continuous tight junctions (Cabezas et al., 2014; Jia, Martin, Zhang, & Jiang, 2013).

Following extravasation, most tumor cells die while others can migrate in the leptomeningeal space or along the blood vessels, and proliferate to form micro-metastases (2% of the circulating tumor cells) (Luzzi et al., 1998; Vanharanta & Massagué, 2013).

They could also lie dormant by entering a slow cell-cycling state through expression of stemness-associated transcription factors such as SOX2 and SOX9 (Heyn et al., 2006; Malladi et al., 2016).

1.1.3 Non-Small Cell Lung Cancer Brain Metastasis

Lung cancer is the leading cause of cancer-related mortality worldwide (Planchard et al., 2018), in addition to being the most common primary origin of BM (Gavrilovic & Posner, 2005). Between 75-85% of patients that experience lung cancer are diagnosed with non-small cell lung cancer (NSCLC) (Kaminski & Krupsky, 2004).

Fortunately, extensive molecular profiling has enabled knowledge of biomarkers and targeted therapies for NSCLC. Chen *et al*. reported that high expression of the vascular endothelial growth factor (VEGF)-C is associated with lung-to-brain metastasis (G. Chen, Liu, Wang, & Liu, 2010). Moreover, the expression of inflammatory chemokines has been implicated in lung-to-brain metastases. The expression of CXC motif chemokine receptor (CXCR4), the receptor of the CXC chemokine ligand 12 (CXCL12), in the primary lung tumor and the associated BM was shown to be higher than that in non-metastatic lung tumors (G. Chen, Wang, Liu, & Liu, 2011). Epidermal growth factor receptor (*EGFR*) mutations and anaplastic lymphoma kinase (*ALK*) rearrangement have also been identified as reliable prognostic markers of lung-to-brain metastasis. In a population-based study, incidence of BM was higher in patients with *EGFR*-mutant NSCLC than those with *EGFR* wild type (39.2 *versus* 28.2%) (Hsu et al., 2016). *EGFR* mutations render BM tumors sensitive to *EGFR* tyrosine kinase inhibitors (TKIs), resulting in significantly improved survival outcomes (Mok et al., 2009; Rosell et al., 2012; Sequist et al., 2013).

As a result of chromosomal rearrangement, a fusion gene consisting of echinoderm microtubule like protein 4 (*EML4*) and *ALK* genes is formed, which codes for a protein with constitutive kinase activity. *ALK* rearrangement is found in approximately 2–7% of NSCLC patients (Kwak et al., 2010; Soda et al., 2007). Since its discovery in 2007, several TKIs have been developed against *ALK*. Despite initial response, resistance invariably develops, which creates the need for more effective and widely applicable molecular NSCLC-derived BM biomarkers.

Recent advancements in whole exome sequencing (WES) have enabled the identification of genomic alterations that promote lung adenocarcinoma brain metastases. In a WES study of 73 patient-derived lung adenocarcinoma BM samples, somatic alterations in the BM cohort were compared to those in a set of 503 primary lung adenocarcinoma samples sequenced by The Cancer Genome Atlas (TCGA-LUAD) to isolate BM-specific mutations from ones also present in primary lung tumors (Shih et al., 2020). Resulting candidate brain metastatic drivers, including amplifications in *MYC, YAP1,* and *MMP13,* were validated using an additional 105 lung adenocarcinoma BM samples. These genes were subsequently overexpressed in PDX intracardiac mouse models and demonstrated a higher rate of lung tumor metastasis to the brain. While this study illustrates a viable pipeline for driver gene signature discovery, its results are inherently limited due to the lack of comparison between the mutational landscape of matched primary lung tumors and BM.

1.1.4 TRAcking Cancer Evolution through therapy/Rx (TRACERx)

The enormous heterogeneity within and between NSCLC tumors hinders the development of a widely applicable prognostic gene signature for lung cancer. Intratumoral heterogeneity is present in many cancer types and is often the limiting factor in driving new therapies. TRAcking Cancer Evolution through therapy/Rx (TRACERx), a whole exome sequencing study, has set out to investigate intratumoral heterogeneity in a prospective cohort of 100 NSCLC patients (Jamal-Hanjani et al., 2017). The TRACERx study evaluates clinical outcomes in relation to genomic alterations, illustrating the clonal nature of driver events and tumor evolutionary trajectories in early-stage NSCLC. The team has also sequenced primary and recurrent metastatic biopsies to address questions of clonality in the context of metastasis and host immune response (TRAcking Cancer Evolution through therapy/Rx (TRACERx) clinical study).

Through our collaboration with Dr. Charles Swanton at The Francis Crick Institute who leads the TRACERx program, we have gained access to several primary lung cancer patient-derived xenografts, which had been propagated *in vivo* for three cycles prior to being handled *in vitro*. We have previously tested CRUK0748 and CRUK0733, tumor samples obtained from two TRACERx patients, in our lung-to-brain metastasis intrathoracic PDX model (Singh, Bakhshinyan, Venugopal, & Singh, 2017) and found that mice injected with CRUK0748 developed BM whereas mice injected with CRUK0733 did not. Interestingly, we later found out that the patient harboring CRUK0748 had presented with brain metastases in the clinic, unlike the patient with CRUK0733 lung tumor, which did not develop BM. Moreover, when the brains of mice injected with CRUK0748 were

harvested at endpoint, cultured, and flow-sorted for a human Tra-1-85 cell population, we saw a population of sphere-forming cells proliferating in CSC-enriching media conditions, possibly showing a stem-like BMIC population. The concordance between patient outcomes and BM in animal models indicates the relevance of the already existing animal model in our laboratory and provides a steppingstone for the development of an orthotopic mouse model suitable for *in vivo* genome-wide screens.

1.2 Animal Models of Cancer Metastasis

Although current pre-clinical models of brain metastasis recapitulate the metastatic cascade and can be engrafted with patient-derived tumor cells, they often present limitations when we need to implant large cell numbers. Below is a review of several experimental models of BM that have been developed. These models are categorized based on tumor origins, as well as the method of tumor metastasis induction.

1.2.1 Syngeneic versus Xenograft

In syngeneic cancer models, immunocompetent mice can be transplanted with tumors derived from mice with the same genetic background, which minimizes the possibility of graft *versus* host disease. While these models keep the microenvironmental and immunological factors in play and follow a disease progression trend analogous to the human counterpart, the transplanted tumor is derived from a non-human organism and limits the conclusions that can be translated to human biological systems. In addition, using commercial human cancer cell lines is suboptimal as they often do not retain the characteristics of the original tumors upon extensive *in vitro* passaging. Patient-derived xenograft (PDX) models use tumor cells from patient biopsies or resections, which are then

engrafted into immunocompromised/athymic mice. PDX models offer the opportunity to investigate biological pathways relevant to human health. The downside of patient-derived xenograft models is the lack of an immune system, which has been remedied by the usage of humanized mouse models (Ito, Takahashi, Katano, & Ito, 2012).

1.2.2 Ectopic versus Orthotopic

Another classification of mouse models in cancer research is ectopic *versus* orthotopic tumor implantation systems. Especially important in metastatic studies, the location of tumor implantation determines the take-rate and the tumor spread capacity. Ectopic tumors are injected in a location other than the primary source of the tumor—often the hind leg (flank) of the mice—whereas orthotopic tumors are implanted in the organ corresponding to the original tumor tissue. Chen *et al.* conducted a CRISPR-Cas9 screen in a mouse model of metastasis where they implanted non-metastatic lung cancer cells subcutaneously and monitored metastasis to the lungs upon the introduction of a knockout library (S. Chen et al., 2015) **(Figure 2A).** While ectopic models minimize trauma and potentially lengthen survival, they ignore the primary tumor microenvironment. Orthotopic mouse models provide more accurate representation of metastasis, as the primary microenvironment of tumor cells plays a role in the upregulated or downregulated genetic programs upon entering circulation. Our laboratory has previously developed pre-clinical PDX BM mouse models that recapitulate BM from lung, breast, and skin cancers through intrathoracic, mammary fat-pad, and subcutaneous injection routes respectively (Singh, Bakhshinyan, et al., 2017) **(Figure 2B)**.

In another study, orthotopic mouse models of lung cancer were developed where tracheal intubation of the lungs was performed during and after injection to prevent lung collapse (pneumothorax) (Nakajima et al., 2014) **(Figure 2C)**. This approach can be taken in developing new lung-to-brain metastasis mouse models when implanting large numbers of lung cancer cells to ascertain the location of tumor inoculation and minimize trauma to the mouse. Tumors whose tissues of origin support basic life functions, such as the lungs, may present as an obstacle when induced with tumors in immunocompromised mice. Fine-tuning of experimental techniques will ensure the optimization of *in vivo* approaches in large-scale studies and maximize the clinical relevance of results.

1.2.3 Intravenous Tumor Induction

As a large portion of cancer cell migration involves mobilization in the circulatory system, seeding tumor cells directly into circulation has been employed as a technique to study metastasis *in vivo*. In a study of NSCLC metastasis to the brain, Yoshimasu *et al.* injected a highly brain-metastatic subclone of lung tumor cells in both the tail vein (intravenous) and the left heart ventricle of the heart (intracardiac) (Yoshimasu et al., 2004). Intracardiac inoculation was used because tumor cells from lung cancer lesions can easily drain into the left ventricle through the pulmonary vein, deeming this injection route clinically relevant.

1.3 Functional Genomics as a Tool to Uncover Drivers of Metastasis

Recent advances in gene editing tools have enabled increasingly informative interrogation of the genomic landscape using both loss-of-function (LOF) and gain-of-function (GOF) gene manipulation methods. The CRISPR-Cas9 (Clustered Regularly

Interspaced Short Palindromic Repeats-CRISPR Associated protein 9) system was shown by Jinek *et al.* to provide bacteria with adaptive immunity against viruses and plasmids by using CRISPR RNA (cRNA) as a guide to silence invading nucleic acids (Jinek et al., 2012). CRISPR and its derivative systems present a unique opportunity for studying cancer-driving genes from a functional standpoint **(Figure 3A)**. Previously, CRISPR knockout studies have identified genes essential for survival of tumor cells, as well as regulators of tumor suppressors or oncogenes. The ability to design custom libraries of single-guide RNAs (sgRNAs) enables simultaneous screening of large collections of genomic elements (coding genes, regulatory elements such as enhancers, noncoding RNAs) in a given biological   context.

1.3.1 CRISPR Activation: Gain-of-Function CRISPR Screens

While LOF studies such as creating insertions/deletions (indels) in the genetic sequence are the hallmark of forward genetics, they focus strongly on essentiality for growth and survival as phenotypes, not fully depicting the intricacies of the metastatic cascade such as invasion, dormancy, or immune-related aspects. Instead, other genetic modulations enabled using the CRISPR system, for instance transcriptional activation (Konermann et al., 2015), can be used when studying cancer metastasis. CRISPR activation (CRISPRa) is an umbrella term representing systems involving a non-catalytic, dead Cas9 (dCas9) protein, alongside a transcriptional activation complex.

Cas9 contains two nuclease domains, RuvC and HNH, that are conserved among several types of nucleases, and each is responsible for cutting one strand of DNA upon binding (Jinek et al., 2012). The catalytic domains can be deactivated by introducing two amino

acid changes (D10A and H840A) to generate dCas9, which is able to connect directly to effector molecules (repressors or enhancers). This deems the dCas9-effector complex an artificial transcription factor that can be guided by the sgRNA to bind to a specific Transcription Start Site (TSS) to activate or repress gene expression, and result in transcriptional activation (CRISPRa) or interference (CRISPRi) (Kampmann, 2018) **(Figure 3B)**. Variations of CRISPRa in eukaryotic cells include dCas9-VP64 or dCas9-p65, VPR, SunTag, and Synergistic Activation Mediator (SAM) **(Figure 3C)**.

The first generation of dCas9 activators in eukaryotic cells included dCas9 fused to the activation domain of p65 or a VP64 activator, an engineered tetramer of the herpes simplex VP16 transcriptional activator domain (Gilbert et al., 2013). The dCas9-VP64 complex performed more effectively than p65 and has been used more commonly.

Another strategy for CRISPR activation, reported by Chavez *et al.*, employs multiple different activators to synergistically amplify activation (Chavez et al., 2015). The authors created a three-part effector system fused to dCas9, comprised of activators V̲P64, p̲65, and R̲ta (VPR). The VPR system activates genes from 5-300-fold at the mRNA level, notably by employing three or four sgRNAs per endogenous gene.

Next, the SunTag system uses dCas9 as a scaffold that can recruit many copies of an activator molecule. The dCas9 protein is linked to a tandem array of peptides called SunTag, through binding scFV (single-chain variable fragment), an engineered portion of an antibody that binds to the SunTag peptides (Tanenbaum, Gilbert, Qi, Weissman, & Vale, 2014). The SunTag peptide array then recruits many copies of VP64, a transcriptional

activator. This enables one dCas9 molecule to recruit up to 24 copies of the scFv-VP64 fusion protein rather than delivering just one VP64 in a dCas9-VP64 fusion setting.

A fourth approach, described by Konermann *et al.* and termed the synergistic activation mediator (SAM) system, employs multiple transcriptional activators through the sgRNA construct to create a synergistic effect (Konermann et al., 2015). Engineered to use first-generation dCas9-VP64, SAM enhances activator recruitment through the addition of an RNA recruiter module, a hairpin from the MS2 bacteriophage, to the sgRNA which interacts with the RNA-binding protein MCP (MS2 coat protein). Moreover, the fusion of MCP to the p65 transcriptional activator as well as to the activating domain of human heat shock factor 1 (HSF1) enhances the activation capacity of the system. The SAM system can increase the activation of endogenous genes on the orders of 2-multiple thousand-fold changes compared to dCas9-VP64.

A variation of the SAM system includes two PP7 aptamers which are derived from the PP7 bacteriophage and recognized by the PP7 Coat Protein (PCP) (Lim, 2002), in addition to the existing MS2 hairpins. This structure leads to the development of a new sgRNA variation called tracr-v14, a design that allows for higher-order combinations of domain recruitment (Sanson et al., 2018). This system was developed due to the low lentiviral titer experienced with using the SAM system containing only the MS2 hairpins. The PP7-MS2 SAM system was used when developing the Human Activation Library (Calabrese, Set A, Addgene #92379) (Sanson et al., 2018), which will be used in this project **(Figure 3D)**.

1.3.2 CRISPR Screens using Animal Models of Cancer and Metastasis

Genome- wide or targeted screens are being used to uncover genomic and regulatory landscapes in oncogenesis, metastasis or drug resistance. These screens lay the groundwork for the discovery of targeted therapeutics against drivers found in the specific patient tumor. Because preclinical mouse models provide highly faithful *in vivo* systems for studying human cancer and therapeutic efficacy, *in vivo* functional genomic studies that can fill this knowledge gap are in high demand (C. Li & Kasinski, 2020).

CRISPR screens in specific harbor the advantage of highly flexible modalities for knockout, knockdown, activation, repression and other perturbations in animal model systems of cancer and metastasis. *In vivo* CRISPR screens have explored questions about tumor growth modulators (Brauna et al., 2016), immunotherapeutic potential of genetic drivers in solid tumors (F. Li, Huang, et al., 2020; Manguso et al., 2017), targetable epigenetic vulnerabilities (F. Li, Ng, et al., 2020), as well as characterization of metastatic drivers in breast and lung cancers (S. Chen et al., 2015; Ebright et al., 2020; Grzeskowiak et al., 2018).

While *in vivo* functional genomic screens can utilize both genome-wide and pooled libraries, it is important to account for the biological phenomenon at hand (e.g. oncogenesis *vs* metastasis) and appropriate animal models when selecting libraries and methods of delivery. Li *et al.* have provided a flowchart that can provide guidance in choosing the appropriate animal model and library design for specific functional genomic research question at hand (C. Li & Kasinski, 2020) **(Supplementary Figure 1)**.

1.4 Statement of Intent

Brain metastases (BM) are the most common tumors of the central nervous system. 40% of patients with non-small cell lung cancer (NSCLC) develop BM, with survival of only 4-11 weeks once diagnosed without treatment, and 16 months with treatment. As systemic therapies for the treatment of NSCLC are becoming increasingly effective at controlling primary disease, patients are ironically succumbing to their BM. This highlights a large unmet need to develop novel targeted therapies for the treatment of lung-to-brain metastases (LBM). Genomic interrogation of LBM using CRISPR technology can inform preventative therapies targeting genetic vulnerabilities in both primary and metastatic tumors. Loss-of-function studies present limitations in metastasis research, as knocking out genes essential for survival in the primary tumor cells can thwart the metastatic cascade prematurely. However, gene overexpression using CRISPR activation (CRISPRa) has the potential for overcoming dependencies of gene essentiality. In this thesis, we hypothesized that by harnessing the power of *in vivo* functional genomics screening in a relevant murine model of lung cancer BM, we can identify druggable targets with translational potential to improve the survival of NSCLC patients. We specifically proposed an *in vivo* genome-wide CRISPR activation screen to identify novel genes, that when overexpressed, drive LBM. To the best of our knowledge, this study is the first *in vivo* genome-wide CRISPRa screen to identify novel drivers of LBM and can inform future preventative therapies to improve survival outcomes for NSCLC patients.
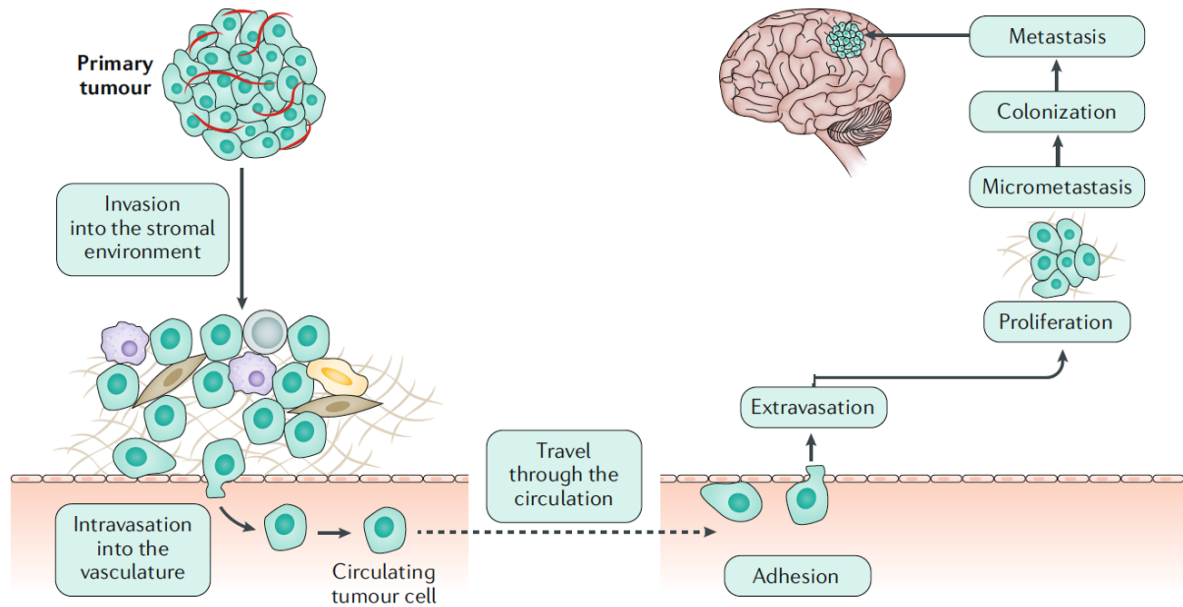
Figure 1. The brain metastatic cascade. As primary tumor cells break off into the circulation, there are several bottlenecks to be overcome prior to the establishment of a brain macrometastasis, such as surviving the sheer force of the circulation, extravasation into the brain, and downregulating/upregulating adaptational pathways to find the brain microenvironment habitable (Achrol et al., 2019)
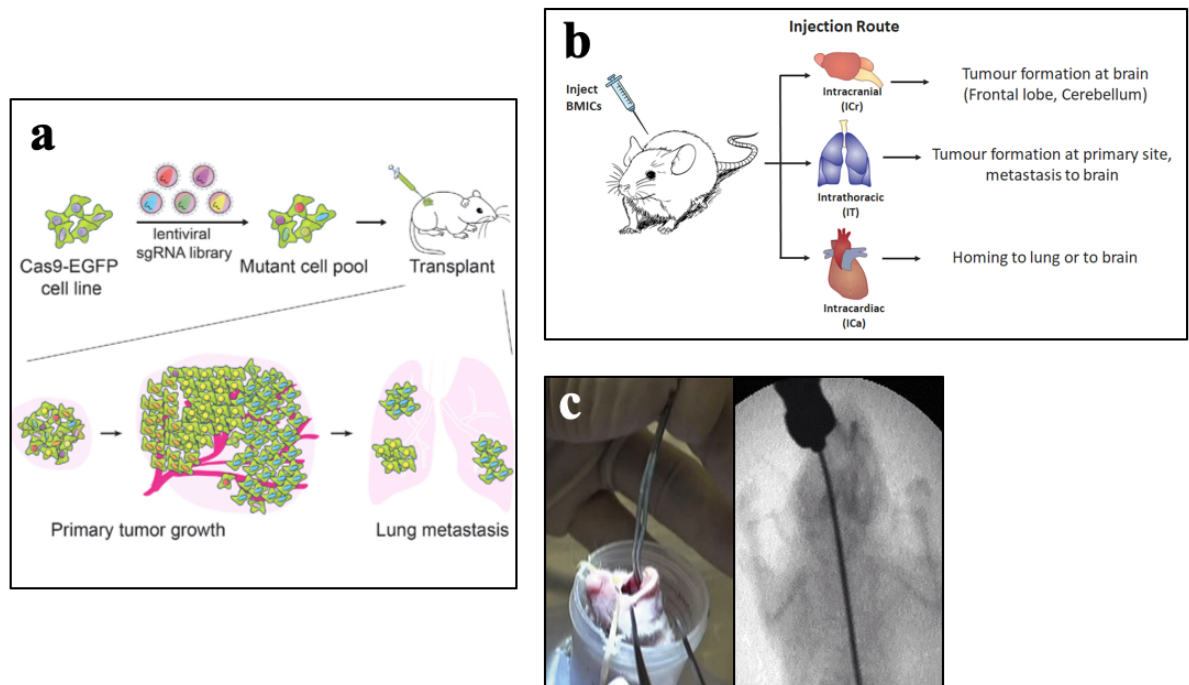
Figure 2. Murine models of metastasis. a) Schematic of a genome-wide CRISPR-Cas9 knockout screen in a mouse model of tumor growth and metastasis (Chen et al., 2015). **b)** Pre-clinical PDX brain metastasis mouse models recapitulating BM from lung, breast, and skin cancers through intrathoracic, mammary fat-pad, and subcutaneous injection routes respectively (Singh et al., 2017). **c)** Orthotopic mouse models of lung cancer using tracheal intubation of the lungs (Nakajima et al., 2014).
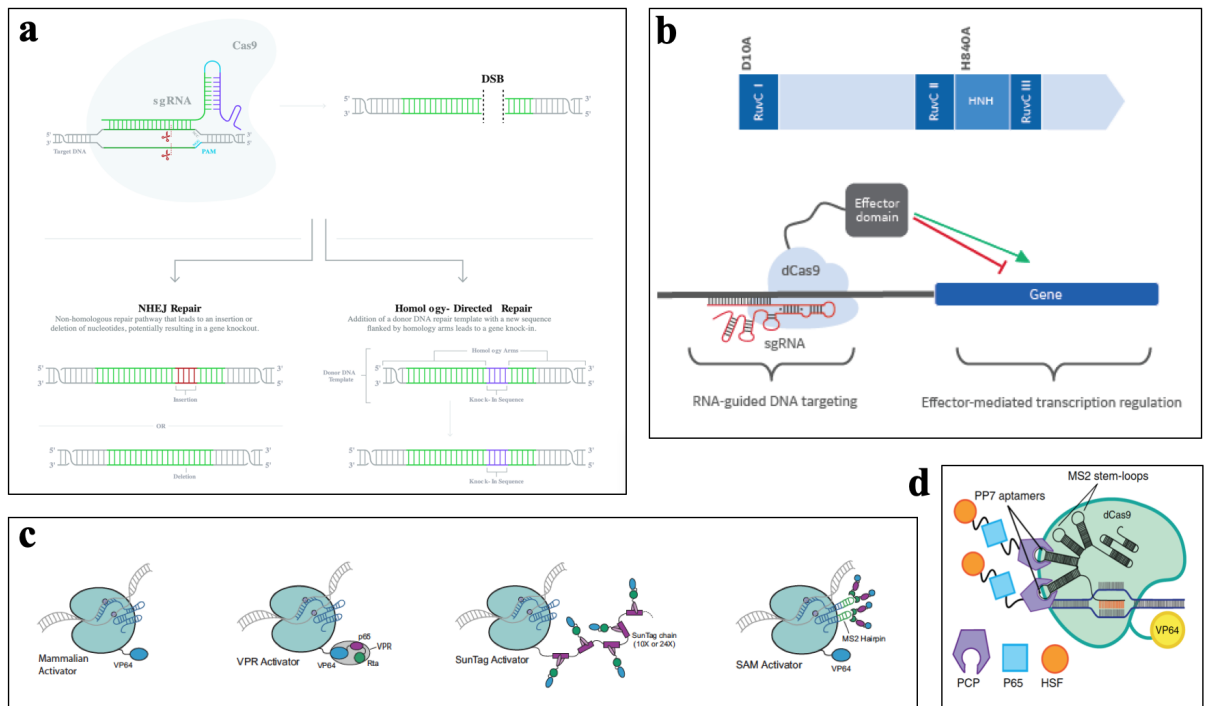
Figure 3. CRISPR knockout, activation, and interference systems. a) The CRISPR-Cas9 knockout screen mechanism. Double stranded breaks (DSBs) are repaired through 1) non-homologous end joining resulting in insertions or deletions (indels) and ultimately a gene knockout, or 2) homology-directed repair (HDR), where a donor DNA repair template is incorporated in the double stranded break. **b)** Schematic of CRISPRa and CRISPRi (CRISPRi) ("What is CRISPRa or CRISPR activation," n.d.). **c)** CRISPRa systems in eukaryotic cells, in the following order: dCas9-VP64 or dCas9-p65, VPR, SunTag, and Synergistic Activation Mediator (SAM). **d)** Schematic of the Calabrese CRISPRa components (La Russa & Qi, 2015).
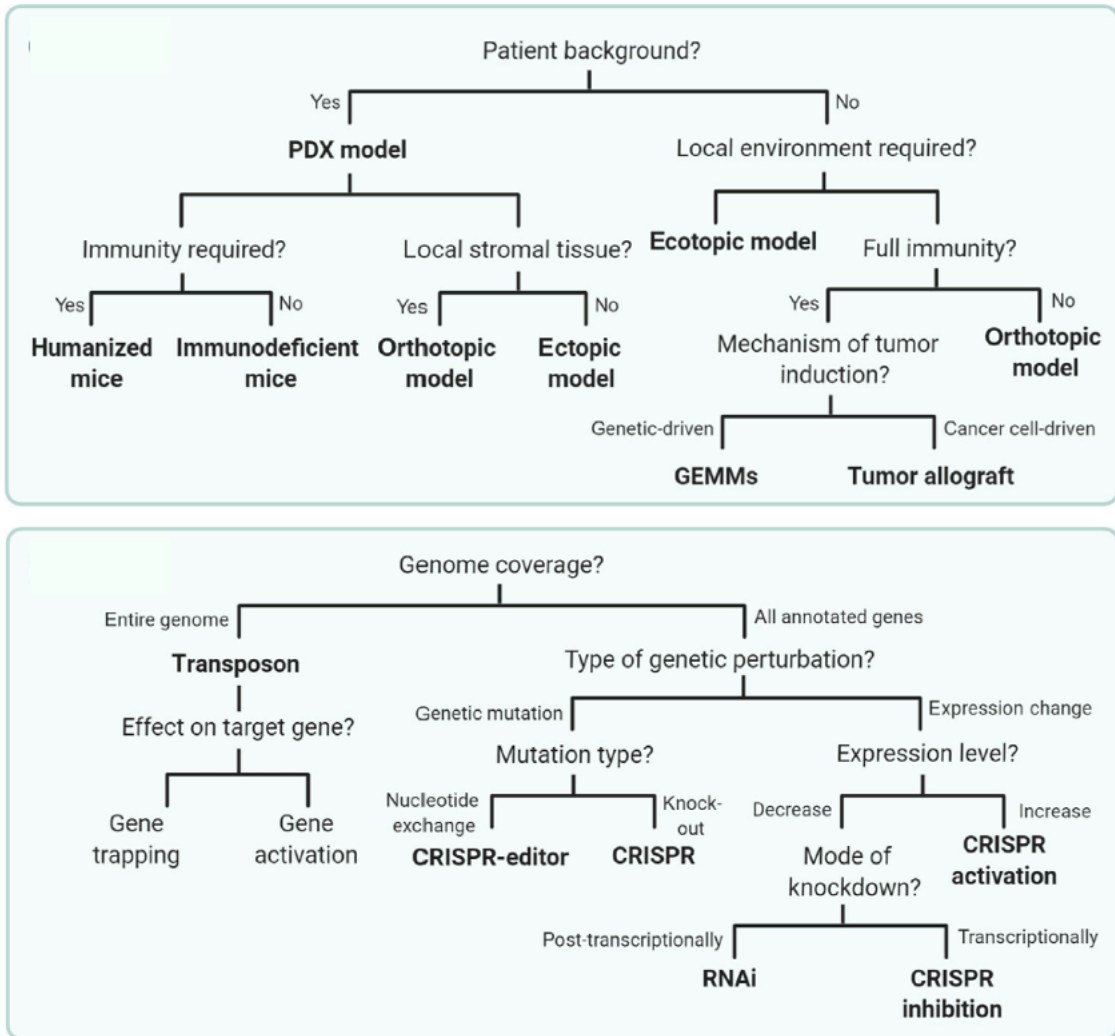
Supplementary Figure 1. Steps to decide on selecting appropriate mouse model and genetic tools for functional *in vivo* interrogation (C. Li & Kasinski, 2020).

CHAPTER 2: Development of an orthotopic PDX murine model of NSCLC to brain metastasis

The goal of this aim was to develop a reliable orthotopic Patient-Derived Xenograft (PDX) mouse model of lung-to-brain metastasis by direct injection of GFP-luciferase CRUK0748 (metastatic NSCLC) and CRUK0733 (non-metastatic NSCLC) cells into the lungs of NSG mice to assess the kinetics of primary lung tumor growth and metastasis to the brain and other organs, through imaging with bioluminescent *in vivo* imaging (IVIS).

2.1 Materials and Methods

2.1.1 Primary Tumor Cell Propagation

CRUK0748 and CRUK0733 have been acquired from Dr. Charles Swanton's in the form of frozen PDX samples, propagated *in vivo* subcutaneously for three cycles immediately after surgical resection. These patient-derived NSCLC cells were obtained as part of our collaboration with Dr. Charlie Swanton's laboratory at the Crick Institute in the UK through his TRACERx study database of genetically annotated NSCLC cells sampling patients from the time of diagnosis to relapse, creating a genomic landscape of changes through space and time that contribute to treatment resistance and development of metastatic disease (TRAcking Cancer Evolution through therapy/Rx (TRACERx) clinical study). Through this collaboration, we initially obtained a NSCLC cell line from a patient who did not develop brain metastasis (CRUK0733) as well as a cell line from a patient with a confirmed brain metastasis (CRUK0748). Whole exome sequencing of these cell lines demonstrated differential expression of tumor suppressors and oncogenic driver mutations, with the non-metastatic CRUK0733 line harboring mutations in *TP53* while the pro-

metastatic CRUK0748 line harbors mutations in both *TP53* and *KRAS*, likely accounting for the more aggressive nature of the CRUK0748 line **(Supplementary Figure 3B).**

The tumor sections provided by Swanton lab were propagated three more times subcutaneously at Singh laboratory, and human cells were isolated using a pan-HLA antibody (HLA-ABC Monoclonal Antibody (W6/32), eBioscience 17-9983-42) by flow cytometry. Cells were then expanded adherently in 50:50 DMEM/F12 (Dulbecco's Modified Eagle Medium/Nutrient Mixture F-12, Thermofisher Scientific #10565018) supplemented with 10% Fetal Bovine Serum (FBS, Wisent Bio Products), 20ng/mL epidermal growth factor (EGF), 10ng/mL fibroblast growth factor (FGF), and 0.1% heparin, maintained at 37°C with a humidified atmosphere of 5% CO2.

2.1.2 Tumor Implantation

Approximately 2×10^6 dCas9-VP64-GFP-Luc+ NSCLC cells expressing the genome-wide Calabrese CRISPRa library (Set A, Addgene #92379) suspended in 63µL of sterile PBS and 7µL of Matrigel were transplanted into the lung parenchyma of 30 immunocompromised NOD Scid Gamma (NSG) mice (4-6 weeks old) for each screen replicate. We have calculated that we will need to inject $\sim 30 \times 10^6$ cells in total to maintain 500X representation *in vivo*, as the library has 56,672 guides and to achieve 500X coverage at least 30 million cells need to be engrafted. Injecting a total of 50×10^6 cells across one technical replicate will theoretically buffer for cell death due to the procedure.

Mice were deeply anesthetized *via* gas anesthesia (Isoflurane: 5% induction, 2.5% maintenance) prior to incision. The skin over the right chest was sterile-prepped using betadine and ethanol mixture and sterile-draped for surgery. A one-centimeter skin incision

was made along the intercostal area and spread apart using a small retractor. A lengthwise incision was made through the pleural cavity to expose the right middle lobe. Varying numbers of cells were slowly injected into the right middle lobe under direct vision using a 32-gauge Hamilton syringe with a blunt end needle at a depth of 5 mm into the lung parenchyma. The right middle lobe of the lung will be allowed to fall back into the pleural cavity and the skin will be closed using interrupted 4-0 Ethicon nylon sutures (Fushiki et al., 2009).

2.1.3 Post-Surgical Monitoring for Formation of Brain Metastases

Mice will be imaged at various time points post-surgery using bioluminescent IVIS imaging to screen for any bioluminescence signal in the primary injection site, the brain, and other organs *in vivo*. Mice will be anesthetized *via* isoflurane and injected intraperitoneally with 10μL/g of a 100X D-luciferin solution (1:2 mixture of 200X D-luciferin in Phosphate Buffer Saline (PBS)). After 10 minutes, the mice will be placed inside of the IVIS machine and images will be taken using the Living Image® software. Cohorts of mice will be sacrificed at different time points based on the intensity of the signal that defines endpoint due to lung tumor burden. Currently, our timepoint experiments demonstrate that mice injected with 1-3.5 million CRUK0733 and CRUK0748 cells may display primary lung tumor signal starting at three days post-surgery. Mice injected with CRUK0748 develop brain metastases at less than a month, while CRUK0733 mice do not. When mice reach endpoint, determined by intensity of lung tumor bioluminescent signal, respiratory or neurological symptom observation, lungs and brains and associated tumors are harvested, along with any extracranial tumors. A subset of matched brain and lung

tissue samples are dissociated enzymatically into a cell suspension and the genomic DNA will be prepared for Next Generation Sequencing to identify guides enriched in both primary and secondary tumors.

2.2 Results

2.2.1 Intrathoracic Injection Route Optimization

To develop a murine model of NSCLC to brain metastasis that can be reliably used in conducting functional genomics screens, we iterated on a previous intrathoracic mouse model developed within Singh laboratory. This model facilitates the engraftment of up to 5×10^5 tumor cells injected in the right upper chest of 8-10 weeks old mice (Singh, Venugopal, et al., 2017). The limitation in this model that needed to be overcome to develop a suitable model for genome-wide screens included the need for higher precision in the location of tumor cell injection in the lung parenchyma (to prevent cell spillage in the pleural space), which directly impacted the maximum number of cells that could engraft effectively in the mouse lungs (primary tumor site). The number of cells injected can play a large role in the time it takes for engraftment. A larger cell number injected may permit for a shorter incubation period, however this may not accurately represent the slower growth observed with the clinical presentation of metastatic progression and it may also result in lost cells during injections due to the sheer injection volume. Conversely, a low cell number may not be engrafted easily, reducing the success rate of engraftment or cell collection (Francia, Cruz-Munoz, Man, Xu, & Kerbel, 2011).

In our newly developed model, lung tumor engraftment was confirmed *via* IVIS three days post-surgery **(Figure 4)**. When testing the tumor progression and metastatic trajectory

of the brain metastatic NSCLC line, CRUK0748 GFP-Luc[+], through this model, we observed that mice succumbed to primary lung tumor burden in approximately 21 days, showing distressed respiration, reduced overall body condition, and reduced activity. Upon *ex vivo* IVIS imaging of the brain, we were able to visualize focal signals in the brains of CRUK0748-injected mice **(Figure 5A)**.

After successfully recapitulating brain metastases in the newly developed intrathoracic injection murine model using a brain metastatic patient-derived NSCLC line, we introduced a second NSCLC line, CRUK0733 GFP-Luc[+], which did not metastasize to the brain in the patient. Upon injection of the same number of cells as used in the metastatic model using non-metastatic NSCLC cells, the primary lung tumor engrafted successfully **(Figure 5B)** but there were no brain metastases detected *in vivo* or *ex vivo* by endpoint. This demonstrated that our intrathoracic NSCLC-BM model was able to recapitulate the brain metastatic cascade from a metastatic patient-derived primary lung tumor, as well as model the absence of brain metastases in a non-metastatic patient-derived NSCLC line.

2.2.2 Injection Cell Number and Engraftment Rate Optimization

The next step in optimizing an animal model suitable for conducting *in vivo* functional genomic screens was to identify the maximum injectable cell number range that could yield maximum primary lung tumor engraftment while enabling brain metastases in a patient-derived metastatic NSCLC cell line, CRUK0748. Through a series of engraftment rate injections, we assessed the degree of primary lung tumor engraftment in mice one week post-injection by injecting 10×10^6, 25×10^6, and 50×10^6 CRUK0748 GFP-Luc^{+} cells in order to find the ideal number(s) of cells that could be engrafted to a level that can represent

a genome-wide CRISPR library *in vivo*. Based on previous lung tumor engraftment analysis on this model, lung tumor signal was present on IVIS after 3 days post-injection. Therefore, the one week timeline was chosen to ensure that initial stages of engraftment would have occurred by the time mice were sacrificed.

We initially intended to inject the entire cell population needed to represent a full CRISPRa library into one mouse to recapitulate the tumor development trajectory seen in the clinic, as well as contain all CRISPRa guides in one biological system to be able to maintain 500X coverage in the tumor cell population being injected (S. Chen et al., 2015). and increase technical replicates by repeating the process in additional mice. In order to fully represent the CRISPRa library in one mouse lung tumor, at least $30x10^6$ NSCLC cells infected with the CRISPRa library lentivirus needed to engraft post-injected. Therefore, we chose a lower, mid-range, and higher cell number ($10x10^6$, $25x10^6$, and $50x10^6$ cells respectively) to assess tumor cell behaviour and engraftment in a variety of injection cell densities. One week after intrathoracic injections, we were able to visualize lung tumor signal in the mice *in vivo*, which corresponded with the *ex vivo* bioluminescent signal in the harvested lung as well **(Figure 6)**. No signal was detected in the brain **(Figure 6)**, which was expected as one week does not allow enough time for lung tumor cells to metastasize to the brain.

Harvested lungs and lung tumors were processed into single cell suspension and prepared for flow cytometry. Flow cytometry was chosen as a method to assess the percentage of human cells present in primary tumor engraftment site, which would allow us to compare number of cells injected with an approximate number of cells that engrafted

after one week. Subsequent flow cytometric analyses to detect the GFP+ human tumor cell population in processed lung and lung tumor samples indicated a 0.22%, 0.33%, 1.93% GFP+ cell population in mouse lungs injected with 10×10^6, 25×10^6, and 50×10^6 cells respectively **(Figure 6)**. GFP+ percentages were converted into approximate cell numbers based on the number of cells injected. Thus, this experiment demonstrated that out of 10×10^6, 25×10^6, and 50×10^6 cells injected, the number of tumor cells that successfully engrafted one week post-injection are 1.45×10^6, 2.75×10^5, and 2.37×10^5 cells respectively. The downward trend in engrafted cell number indicates that increasing initial cell numbers to be injected has a negative impact on engraftment rates. The results of this experiment illustrated the limitation in implanting high tumor cell numbers in one mouse lung for the purpose of containing the entire CRISPRa library in one biological system (one mouse).

2.2.4 Mouse Model Monitoring, Endpoint Determination, and Suitability for CRISPR Activation Screening

Based on the tumor development trends observed through both imaging and mouse behaviours/conditions during the animal monitoring period, we identified an endpoint of 3-4 weeks for metastatic NSCLC and >5 weeks for the non-metastatic NSCLC model. Interestingly, CRUK0748 (metastatic) showed not only a higher propensity to metastasize to the brain, but also displayed more tumorigenicity at the primary site compared to CRUK0733 (non-metastatic) **(Figure 5)**.

Transitioning into Chapter 3 which encompasses the genome-wide CRISPR activation screen to study the effects of gene activation on NSCLC-BM formation, we decided to perform an *in vivo* genome-wide CRISPRa screen using our established CRUK0733 GFP-

Luc$^+$ and CRUK0748 GFP-Luc$^+$ PDX NSCLC mouse models (i.e. both non-metastatic and pro-metastatic lines). The intrathoracic surgical model developed in Aim 1 showed the capacity to accurately recapitulate the occurrence and absence of brain metastasis using metastatic and non-metastatic patient NSCLC samples respectively. Performing screens in both non-metastatic and pro-metastatic models would ensure success of obtaining hits just in case mice succumb to lung tumors before they develop metastasis or if mice do not ultimately develop brain metastasis while screening in a non-metastatic line.

2.2.5 Short-Term Next Steps

A valuable avenue to continue characterizing the animal model discussed in this chapter is to further validate the pre-clinical relevance of this PDX model using other patient-derived cell lines, including additional non-metastatic and metastatic CRUK lines. Moreover, through collaboration with Dr. Shargall, who will kindly provide our laboratory with patient-derived lung tumor samples, we can develop new NSCLC primary cell lines and evaluate our model through capturing similarities and differences in tumorigenesis and metastasis compared to the clinical trajectory of the patients.
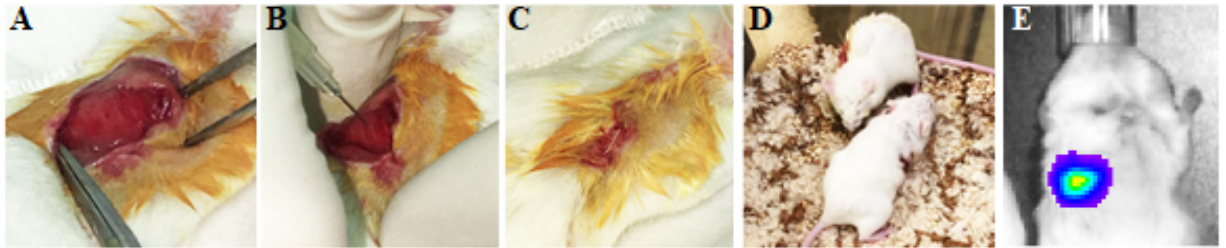
Figure 4. Direct intrathoracic injection of patient-derived lung cancer cells. A) Right-sided thoracotomy exposes the rib cage and underlying pleural cavity and lung. **B)** Injection of 50 million GFP-Luc CRUK0748 NSCLC cells into the right middle lung lobe. **C)** Thoracotomy wound closure using sutures. **D)** Post-operative recovery without any morbidity and mortality. **E)** Bioluminescence imaging 3 days post-injection shows focal intrathoracic tumor signal.
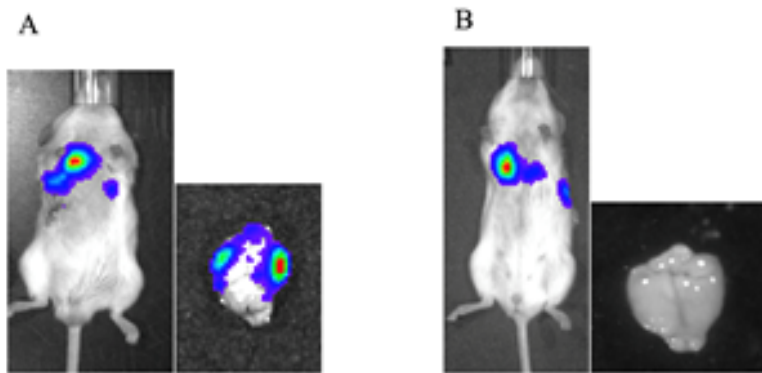
Figure 5. Detecting lung tumor and brain metastases formation using *in vivo* and *ex vivo* bioluminescent imaging. **A)** A mouse that received intrathoracic injection of pro-metastatic CRUK0748 NSCLC cells developed lung and brain tumor burden after one month, whereas **B)** a mouse that received injection of non-metastatic CRUK0733 NSCLC cells did not form brain metastases.
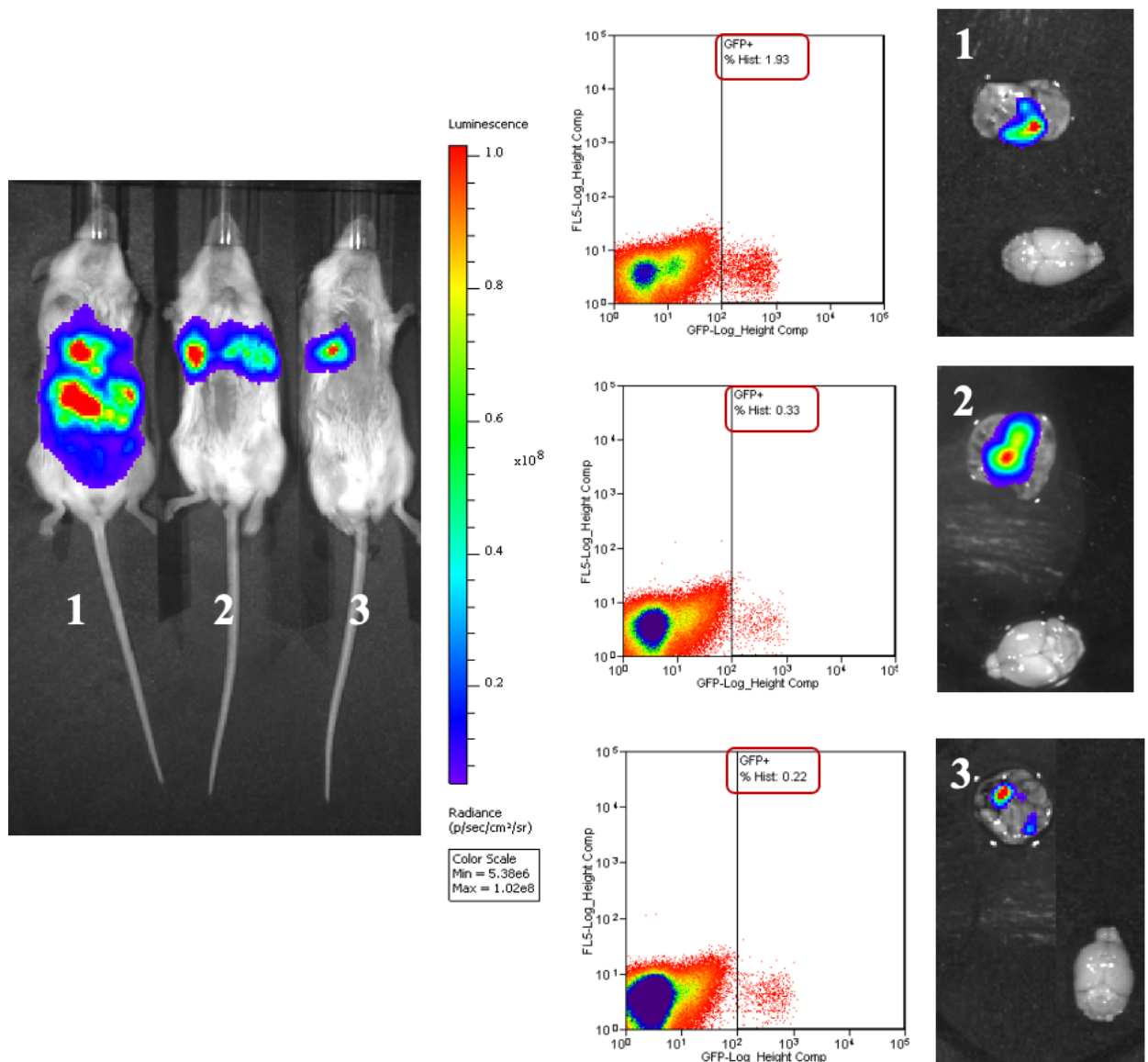
Figure 6. Engraftment Rate Experiments to Characterize Intrathoracic LBM Model with CRUK0748 **Cells.** Mice injected with 50 million (mouse #1), 25 million (mouse #2), and 10 million (mouse #3) CRUK0748 GFP-Luc cells were sacrificed one week post-injection. *In vivo* bioluminescent lung tumor signals were captured (left image), and lungs/lung tumors were analyzed for GFP+ human tumor cells *via* flow cytometry (middle panel). Each mouse's lung and brain were imaged *ex vivo* (right panel of three images) to visualize any lung tumors and brain metastases.

CHAPTER 3: Conducting an *in vivo* genome-wide CRISPR activation screen in a PDX orthotopic mouse model of NSCLC-BM

The power of an *in vivo* CRISPR activation (CRISPRa) screen for the purpose of elucidating drivers of LBM are several-fold: 1) By studying gene activation (a positive selection screen) versus inhibition (a drop-out screen), we can identify genes, that when upregulated, drive LBM formation; 2) *In vivo* screening more faithfully recapitulates the human disease for increased translational accuracy compared to *in vitro* screening; and 3) An *in vivo* screen allows for the study of metastasis formation in the context of a tissue microenvironment. Recently, a group performed a genome-wide CRISPRa screen in a mouse model of breast cancer metastasis, demonstrating the feasibility of using the CRISPRa platform for *in vivo* functional genomics screening (Ebright et al., 2020). The goal of this aim was to conduct a genome-wide CRISPR activation screen in a PDX mouse model using non-small cell lung cancer to identify drivers of lung-to-brain metastasis.

3.1 Materials and Methods

3.1.2 CRISPRa Library Viral Generation and Cell Characterization

3.1.2.1 Library Amplification

We first electroporated the library using Endura electrocompetent cells (Lucigen, #60242-1) by setting up a total of 4 electroporations, each containing 2μL of 50ng/μL of the Human Calabrese CRISPR activation pooled library Set A (Addgene #92379) and 25μL of thawed Lucigen Endura electrocompetent cells, added to pre-chilled cuvettes (1.0 mm) on ice. Electroporated cells were flushed out and pipetted up using 975μL of Recovery Medium (Lucigen, #80026-1) and transferred to a culture tube with an additional 1 mL of

Recovery Medium. Tubes were placed in a shaking incubator at 250 rpm for 1 hour at 37°C. Next, all four tubes were pooled in one 15 mL falcon tube and mixed well. To set up a dilution plate, 10μL of the pooled cells were added to 990μL of Recovery Medium for an 800-fold dilution. 20μL of the dilution mixture was plated onto a pre-warmed 100 mm LB-ampicillin (100 mg/mL) agar plate. This resulted in a 40,000-fold dilution of the full transformation that would be used to calculate the transformation efficiency.

The library was plated and grown on 40 agar plates, where 200μL of the recovered cell mixture was plated on each of the 40 pre-warmed 150 mm LB-ampicillin (100 mg/mL) agar plates using plastic spreader sticks. Plates were incubated for 14-16 hours at 30°C. Growth at this lower temperature minimizes recombination between long-terminal repeats.

Next, we harvested colonies after 14-16 hours by using 7 mL of LB-ampicillin to scrape off the colonies into a sterile flask, and 5 mL to rinse the plates afterwards.We incubated the flask containing colonies from the 40 agar plates while stirring at room temperature for 1-2 hours. We then centrifuged the bacterial culture at 4°C, 7000 x g for 10 minutes and weigh the wet pellet **(Figure 7A)**. Plasmid DNA was purified using a maxi- or mega-scale plasmid purification kit and DNA yield was quantified using NanoDrop UV spectrophotometry. Prior to infecting cells with the library, Next Generation Sequencing (NGS) was performed on the pooled CRISPRa library plasmid to confirm library representation **(Figure 8)**.

3.1.2.2 Calculating transformation efficiency

We counted the number of colonies on the 40,000-fold dilution plate and multiplied the number of colonies by 40,000 to obtain the total number of colonies plated. In this study,

in order to reach 500X library coverage (56,762 sgRNAs), we need 56,762 x 500 = 28,381,000 colonies in total. Thus, we proceeded if the total number of colonies fulfills the required number. Obtaining sufficient number of colonies ensures full library representation is preserved.

3.1.2.3 CRISPRa Library Quality Control and Lentiviral Generation

For library plasmid pool quality control, the plasmid is digested by the single-cutter enzyme BamHI and ran on a 2% agarose gel to determine whether it corresponds to the correct plasmid weight **(Figure 8A)**. Additionally, 50ng of CRISPRa library plasmid is sent along with P5 and P7 primers to Donnelly Sequencing Centre in Toronto for NGS on Illumina NextSeq (Broad Institute Sequencing Protocol). Sequencing results were analyzed using the MAGeCK pipeline (W. Li et al., 2014) (alignment to library), and a Cumulative Distribution Function (CDF) plot was created to determine how close the value of the area under the curve (AUC) is to 0.5.

The CRISPRa Calabrese plasmid pool (Set A, Addgene #92379) is used to produce lentivirus, using the packaging protocol outlined in Sanson *et al* (Sanson et al., 2018). In short, twenty 150mm dishes of 80% confluent HEK293T cells (~12 million cells) are transfected with VSVG (4.2 ug), Gag/Pol (42 ug), library plasmid pool (33.3 ug), and Xtremegene 9 (238.5 uL), and mixed it in a total of 2 mL OptiMEM and added to each plate of HEK293T cells. Three rounds of viral soup are harvested over days 2-4. On day 5, viral particles are pelleted *via* ultracentrifugation, and concentrated virus was stored at 4 degrees overnight, followed by long-term storage at -80 degrees Celsius.

3.1.2.4 Puromycin Kill Curve

The library pool plasmid contains a puromycin resistance cassette which enables *in vitro* selection post-infection to achieve a cell population that have successfully integrated guide RNA plasmids. In order to determine the minimum inhibitory concentration (MIC) of puromycin that will eradicate 100% of cells with no sgRNA plasmid in 48-72 hours, we use the following protocol on CRUK0733 GFP-luc dCas9-VP64 cells:

1.   Add 1.92 µL of 10 mg/mL puromycin to 3000 µL of cell culture media.

2.   Perform a serial dilution by adding 1.5 mL of puromycin-containing media to 1.5 mL of puromycin-free media until you reach a [puro] of 0.1 µg/mL.

3.   Add 200 µL of each dilution (plus control) per well to a 96-well TC-treated plate with 6 technical replicates per concentration.

4.   Sort 1000 live cells per well and include 2 wells with no cells as control (blanks).

5.   After 48 hours, perform a visual check to determine number of cells viable in each concentration.

6.   Determine a range of antibiotic concentrations that led to cell death after counting cells visually. These concentrations will be used in a secondary study using a hemocytometer to determine number of cells viable in a 6-well dish experimental format (3 technical replicates per concentration).

7.   Draw up a dose-response curve and determine the minimum inhibitory concentration (MIC) of puromycin.

8.   Confirm MIC by plating cells at a confluence and plate size of your choice.

3.1.2.5. Determining Cell Doubling Time

For adherent cultures such as CRUK0733, we plate 10 million cells in two 150 mm dishes and inspect cells after 2 days to estimate confluence. When plates reach ~90% confluence, we count cells using Trypan Blue and calculate doubling time using the following equation:

No. of live cells at endpoint/No. of live cells plated = X

log2(X) = Y

Y/No. of days elapsed = doubling time in days

3.1.2. dCas9 Activity Assay

To confirm the expression and functionality of dCas9 protein transduced into CRUK0733 GFP-Luc cells, we utilized the Broad Institute dCas9 Activity Assays for adherent cells. We acquired a CD45-targetting single guide RNA (sgCD45) plasmids from the Broad Institute. We then generated lentivirus and infected CRUK0733 GFP-Luc cells with sgCD45 virus in 6-well plates in technical duplicates. After one week of puromycin selection, flow cytometric analyses were performed to determine changes in expression levels of CD45.

3.1.2.7 Data Analysis

Distribution of the p-values will be calculated using a hypergeometric distribution equivalent to a one-sided Fisher's exact test for the top ten genes differentially enriched in the brain metastatic lesions as opposed to the lung tumor. CRISPRa plasmid pool sequencing results are analyzed using the MAGeCK pipeline (alignment to library) and creating a Cumulative Distribution Function (CDF) plot to determine how close the value of the area under the curve (AUC) is to 0.5.

Upon extraction of mouse tissues after mice reach endpoint, gDNA will be extracted from individual tissue samples (individual brain, lungs/lung tumors from each mouse) and sequenced separately. Sequencing library preparation and NGS will be done at Donnelly Sequencing Centre using an Illumina sequencer, and sgRNA abundance determined using published algorithms (Sanson et al., 2018).

Following completion of Illumina sequencing, normalized read counts of guides in each screen will be quantified through quantifying log2 fold change (LFC) of each sgRNA by comparing read-depth-normalized sgRNA counts at the beginning of each screen (T0) to the end of each screen (Tn). T0 signifies the cell population that was directly injected into mouse lungs. To perform quality control analysis, the LFC for all gRNAs targeting a single gene will be averaged, with three sgRNAs targeting each gene in the library. We will repeat the screen in three technical replicates to determine statistical significance of guides that enrich in BM.

3.1.1 Western Immunoblotting

$30\mu g$ of denatured protein per sample was loaded and resolved on SDS polyacrylamide gel, followed by electrotransfer onto PVDF membrane. Membranes were blocked with 3% BSA in 1xTBS (for phosphorylated proteins) and 3% non-fat dry milk in 1xTBS (for normal proteins), incubated with primary antibody at 4°C overnight, then washed and hybridized with Li-Cor IRDye® 800CW Goat anti-Mouse IgG1 secondary antibody and imaged using LI-COR Odyssey Platform. Primary antibodies used included anti-dCas9 (mouse; 1:10,000; Diagenode #C15200203-100) and anti-GAPDH (mouse; 1:40,000; Abcam #ab8245).

3.1.2 Lentiviral Generation

Lentiviruses are generated using the HEK (Human Embryonic Kidney) 293T cell line.

Day 0: On the day before transfection, plate HEK 293T cells in a vessel of choice (e.g. 150 mm plates) such that they are 70-80% confluent on the next day.

Day 1: On the day of transfection, prepare a mixture of two packaging plasmids (pMD2.G and psPAX2) in 1:1 molar ratio in 100µL OptiMEM per plate (Thermofisher, #31985062) and add the required amount of your desired DNA plasmid (library, GFP-luc, or dCas9). Prepare a separate mixture of the transfection reagent, in this case of XtremeGENE 9 (Roche, #06365779001), in a separate tube containing 800µL OptiMEM. Following five minute incubation, add an appropriate amount of plasmid mix to the XtremeGENE 9 mix for a 3:1 ratio of transfection reagent:µg of DNA complex. Add polybrene to the mix at a ratio of 1:500 to increase transfection efficiency. Mix gently and incubate for 20 minutes at room temperature. Next, carefully transfer the transfection mix to the plate of packaging cells. Add entire mix using a 1 mL pipette tip, drop-wise in a circular, zigzag motion without disturbing cell monolayer. Place plates in the incubator and make sure plates are level. Incubate for 24 hours.

Days 2-4: Collect media from HEK 293T plate and store at 4°C. Continue harvesting viral soup for three days post-transfection.

Day 4: After collecting viral supernatant three times (24 h, 48 h, and 72 h), centrifuge the viral suspension at 1000 rpm for 10 minutes, and collect the supernatant. Filter the supernatant through a sterile 0.45-micron SFCA syringe filter (Thermo Fisher, #723-9945) to exclude HEK 293T cells from the viral supernatant. Concentrate the virus through ultra-

centrifugation at 15000 rpm at 4°C for 2 hours. The supernatant is discarded in bleach and each pellet resuspended in any desired volume.

3.1.3 Determining the Viral Concentration for Desired Multiplicity of Infection (MOI)

To achieve a single sgRNA integration per cell, an MOI of ~0.3 was chosen to ensure 30% of transduced cells survive after puromycin selection. A viral concentration that induces puromycin resistance in 30% of cells would be the desired concentration for transducing the recipient cell population in our CRISPRa screen.

While the *in vitro* stage of the CRISPRa screen was performed in 100mm tissue cultured-treated dishes, the MOI experiment was scaled down to 6-well dishes (number of cells seeded, volume of media, and viral volumes were all scaled down by a factor of 5.9 times, based on the difference in surface area of 100mm and 6-well vessels). The viral volume that resulted in an MOI of ~0.3 was multiplied by the same factor, 5.9, to be used in the CRISPRa screen.

Viral dilutions used for each screen depended on the transduction efficiency of the recipient cell line. In the case of the non-metastatic line CRUK0733, viral volumes included 0μL, 4μL, 8μL, 10μL, 15μL, and 20μL per well (total media volume of 1.7mL). For the metastatic line CRUK0748, viral volumes included 0μL, 25μL, 50μL, 75μL, 100μL, and 200μL (two replicates per volume). On day 0, 85000 cells were plated in each well of two 6-well dishes in addition to the associated viral volume and polybrene (1:500 dilution) in puromycin-free media. On day 1, we began puromycin selection on the first replicate of each viral volume and continued selection for four days, while the second replicate of each viral volume remained in puromycin-free media. On day 4, all wells reached confluence

and each well was divided into two. On day 7, cells from all wells were harvested and counted using Trypan Blue Stain (0.4%, Gibco by Life Technologies, REF 15250-061), EVE cell counting slide (NanoEnTek, REF E1020), and the Countess cell counter (Life Technologies). MOI for each viral volume was calculated as the ratio of live cell numbers in puromycin-treated to non-puromycin-treated wells for each viral volume. The viral dilution that yielded a 30% transduction efficiency under puromycin selection compared to the unselected replicate was chosen for each cell line as the appropriate viral volume for CRISPRa screening and was multiplied by 5.9 to be used at a larger scale in 100mm tissue culture vessels.

3.1.4 Genomic DNA Extraction and Quantification

3.1.4.1 Genomic DNA Extraction from Mouse Brain, Lung, and Lung Tumor

For this step, the Gentra Puregene Tissue Kit (Qiagen, #158689) was used and scaled up for our purposes. After mice injected with NSCLC cells infected with the CRISPRa library reach endpoint, brains, lungs, and lung tumors are harvested and processed for downstream gDNA extraction. All physical dissociation steps are done on ice. First, tissue is minced in a 10 cm dish using a sterile razor blade and washed with PBS and transferred to a Dounce homogenizer. Minced tissue is processed in the Dounce homogenizer for 1-2 minutes and transferred to a 50mL Falcon Tube in a final volume of 9mL Cell Lysis Solution which initiates the enzymatic dissociation of tissue. Next, we add 15μL Puregene Proteinase K, mix by inverting 25 times, and incubate on a tube shaker at 55°C overnight. The next day, 45μL of RNase A Solution is added to the Falcon Tube, mixed by inverting 25 times, and incubated on a tube shaker for 60 minutes at 37°C. We then incubate the tube

on ice for 15 minutes, add 3mL Protein Precipitation Solution, and vortex vigorously for 40 seconds on high speed. At this point, solid protein precipitate should be visible. Next, the mixture is centrifuged for 10 minutes at 2000xg. The supernatant is added to 9mL of isopropanol in a fresh 50mL Falcon Tube and homogenized well using a 1mL pipette. The mixture is centrifuged for 5 minutes at 3000xg. The supernatant is discarded carefully and 9mL of 70% ethanol is added to the tube to wash the DNA pellet. The tube is inverted several times to wash the pellet and centrifuged for 3 minutes at 2000xg. The supernatant is discarded carefully, and the pellet is drained and allowed to air-dry on a clean piece of absorbent paper for 10 minutes. The gDNA pellet is then resuspended in 400μL of DNase- and RNase-free water, and the DNA is incubated on a tube shaker at room temperature overnight.

3.1.4.2 Genomic DNA Quantification *via* NanoDrop Spectrophotometer and Qubit 2.0 Fluorometer

To quantify gDNA concentration and purity using NanoDrop 2000/2000c Spectrophotometer, the machine is first blanked with 2μL of DNA sample diluent (water or TE). Next, 2μL of the DNA sample is loaded onto the measurement pedestal. DNA concentration and purity (ratio of absorbance values at 260nm/280nm) will then be shown as outputs. A $A_{260/280}$ value of ~1.8 is normally considered as pure DNA. Abnormal 260/280 ratios usually indicate that a sample is contaminated by residual phenol, guanidine, or other reagent used in the extraction protocol, in which case the ratio is normally low (Wilmington, 2012).

The Qubit dsDNA Broad Range (BR) assay (Thermo Fisher, Q32853) is highly selective for double-stranded DNA (dsDNA) over RNA and is designed to be accurate for initial sample concentration from 100 pg/µL-1000 ng/µL. To prepare samples and standards to be quantified using Qubit Fluorometer, Qubit working solution is prepared by combining 398µL of BR buffer and 2µL of BR reagent in a 1.5mL microfuge tube and vortexed thoroughly. To construct Standards 1 and 2, 190 µL of the Qubit working solution is added to each of two 0.5mL PCR tubes. Next, 10µL of Standard 1 is added to the corresponding Standard 1 PCR tube, and 10µL of Standard 2 is added to the corresponding Standard 2 PCR tube. Mixtures are vortexed thoroughly and incubated at room temperature for two minutes. To prepare gDNA samples, 199µL BR buffer is added to 1µL of BR reagent (for each sample) in a 1.5mL microfuge tube and vortexed to make a working solution. Next, 198µL of working solution is combined with 2µL of diluted gDNA (1:10 in TE) in a 0.5mL PCR tube, vortexed, and incubated at room temperature for two minutes. DNA concentration is then quantified using Qubit Fluorometer.

Comparisons between the selectivity of NanoDrop and Qubit (UV spectrophotometry and fluorometry) in quantifying double-stranded genomic DNA show that when quantifying samples containing both DNA and RNA (such as gDNA extracted from mouse tissue with potential RNA contamination), Nanodrop results are nondiscriminatory, meaning DNA and RNA are not distinguished. On the other hand, Qubit Fluorometers are able to quantify separately the concentrations of DNA and RNA present in a similar sample (Thermo Fisher). Therefore, for quantifying gDNA in this project, we decided to choose Qubit as the primary method of DNA concentration determination.

3.2 Results

3.2.1 Cell line characterization

The recipient cell lines used in the CRISPR activation screens included CRUK0748 and CRUK0733, both of which were transduced with a GFP-luciferase construct, gifted by Dr. Fred Lam **(Supplementary Figure 2),** to enable *in vitro* and *in vivo* tumor cell tracking. Both cell lines were used in separate *in vivo* screens using the intrathoracic PDX model discussed in Chapter 2.

3.2.2 dCas9-VP64 lentiviral transduction and dCas9 activity assay

The CRISPR activation library of our choice, Calabrese (Set A, Addgene #92379), has a two component catalytically dead Cas9 nuclease (dCas9) conjugated to the VP64 transcriptional activator cofactor (dCas9-VP64) and a target sgRNA lentiviral plasmid transduction system that has been optimized for screening in difficult to culture patient-derived cell lines (Sanson et al., 2018). The dCas9-VP64 binds to the target gene of interest *via* the sgRNA but unlike wild-type Cas9 endonuclease, dCas9 does not induce a double-strand break in the DNA double helix. Instead, the VP64 transcriptional transactivator recruits other transcriptional cofactors to induce transcription of the targeted gene.

Using lentiviral infection techniques, we infected CRUK0733 and CRUK0748 cells with a dCas9-VP64 vector. After selection with blasticidin, we confirmed the presence of dCas9 through western blotting in CRUK0733 and CRUK0748 **(Figure 9A)**, and the activity of dCas9 in CRUK0733 through a dCas9 activity assay by infecting dCas9-VP64-GFP-Luc CRUK0733 cells with an sgRNA targeting CD45 (Broad Institute). Cells that were infected with sgCD45 were assayed for CD45 overexpression compared to non-

infected cells using flow cytometry. Results showed that over 98% of infected cells demonstrated CD45 expression, and overall demonstrated that we can utilize the CRISPRa platform in CRUK0733 and CRUK0748 dCas9-VP64-GFP-Luc cells **(Figure 9B)**.

3.2.3 CRISPR Activation Library Amplification, Lentiviral Generation, and Determination of Multiplicity of Infection (MOI)

To conduct a gain-of-function genomic screen through transcriptional activation in an animal model of NSCLC-BM, we employed the Doench Lab human Calabrese whole-genome CRISPRa library (Set A, Addgene #92379) which contains 56,762 sgRNA guides targeting 18,885 genes (Sanson et al., 2018). We successfully electroporated and expanded the CRISPRa library in bacteria with colony growth suggesting 500X library coverage assuming that each individual colony grew from one bacterial cell that incorporated one individual sgRNA plasmid (**Figure 8A**). We purified high yield, high quality pooled plasmids (6642.1 ng/μL, $A_{260/280}$=1.94) from these colonies. We then verified the quality and 500X minimum representation of the genome-wide CRISPRa library guides through Next Generation Sequencing (NGS) (Donnelly Centre for Cellular & Biomolecular Research) and downstream analyses pipelines (**Figures 8B-C**).

Upon confirmation of the library plasmid's quality and adequate guide representation, we generated CRISPRa lentivirus using methods described above. We then determined the viral dilution that resulted in a MOI of ~0.3 for both cell lines (CRUK0748 and CRUK0733). MOI is defined as the number of genomes of a given virus species that infects a cell. For multiple constructs (such as in a pooled CRISPR screen), it is important to stay at an MOI of ~0.3 to enable result deconvolution and avoid ambiguity of the results. In a

pooled screen, cells should be transduced at an MOI of 0.3 to maximize the number of cells with a single integration and limit the number of cells needed at transduction.

An MOI of ~0.3 corresponds to the specific viral dilution at which 70% of the cells remain untransduced and should die through antibiotic selection. At an MOI of 0.3 or less, greater than 95% of infected cells are predicted to have a single integration.

Using the MOI determination protocol discussed above, CRUK0733 cells required a viral volume of 50μL per 5×10^5 in 10mL culture media to reach an MOI of 0.3, while CRUK0748 cells required a viral volume of 383.5μL per 5×10^5 in 10mL culture to reach an MOI of 0.3. An interesting observation was that CRUK0733 cells integrated the plasmid at lower lentiviral concentrations than CRUK0748 cells, meaning the CRISPRa lentivirus showed higher transduction efficiency in CRUK0733 **(Supplementary Figure 5)**.

3.2.4. In vitro *infection of NSCLC cells with CRISPR activation library*

To achieve 500X representation of the CRISPRa library, we deduced that we needed a final cell population of minimum 50×10^6 cells infected with the library to be injected into the lungs of 25 mice (2×10^6 cells per mouse lung). Based on a four-day puromycin selection timeline for both CRUK0733 and CRUK0748 cell lines (at puromycin concentrations of 3μL/mg and 4μL/mg respectively), the *in vitro* selection and expansion process spanned over 6-7 days prior to injection. The *in vitro* stage of the CRISPRa screen started with 20 screen plates (CRUK cells + CRISPRa lentivirus), and four control plates (no puromycin + no virus, puromycin + no virus, no puromycin + virus, polybrene only). On day 0, 500,000 CRUK cells were seeded in 100mm tissue culture-treated screen plates with the appropriate volume of CRISPRa lentivirus to achieve an MOI of ~0.3 and polybrene at a

concentration of 1:500. The same number of CRUK cells were also seeded into control plates based on the specific requirements. On day 1, screen plate media was changed on all 20 plates from puromycin-free media to puromycin-containing media. On day 4, all screen and control plates will reach confluence and be split at a ratio of 1:2 plates through enzymatic dissociation. After four days of selection, screen plate media was changed to puromycin-free media for days 5 and 6 to allow cells to recover before dissociation for injection sample preparation. At this point, if the cell population reaches $90x10^6$ cells, we would be able to use $30x10^6$ for harvesting a T0 cell pellet (initial screen timepoint) and frozen at -80°C to be sequenced at a later stage, and $60x10^6$ cells will be used for downstream injection purposes.

3.2.5 Intrathoracic injections of NSCLC cell population containing CRISPR activation library

Subsequent to expanding the CRISPRa screen cell population, ~$60x10^6$ CRUK cells were harvested from screen plates in three batches and prepared in vials of $2x10^6$ cells per mouse in a final volume of 70uL PBS+10% Matrigel. Cells from control plate containing only CRUK cells exposed to neither CRISPRa virus nor puromycin were dissociated and prepared for control injections (three control mice in the CRUK0733 screen and four control mice in the CRUK0748 screen). CRISPRa and control cells were then injected into 30-33 NSG mice (depending on the number of final cell population *in vitro*) *via* the orthotopic intrathoracic injection method discussed in Chapter 2. Mice were monitored until they became sternal and recovered fully from the injection.

3.2.6 Mouse Monitoring, Imaging, and Endpoint Determination

Lung tumor burden and any cranial or extracranial metastases were monitored using regular bioluminescent IVIS imaging. Mice injected with CRUK0733 CRISPRa screen and control cells were imaged at days 5, 26, 32, 41, 55, 69, 78, 86, and 92 (20 mice are alive and nine mice have been sacrificed to this day). Mice injected with CRUK0748 CRISPRa screen and control cells were imaged at days 9, 15, 22, and at endpoint, between days 26-29 (all CRUK0748 mice have been sacrificed).

Overall, CRUK0733 mice displayed a strong initial lung tumor signal but plateaued as more imaging timepoints surveyed lung tumor growth. On the other hand, mice injected with CRUK0748 displayed a consistent increasing trend in lung tumor growth over four distinct timepoints. In both screens, no brain metastases were visible *in vivo*, but all CRUK0748 mice displayed *ex vivo* brain and extracranial metastases signal, unlike the CRUK0733 mice that have been sacrificed and imaged *ex vivo* to this day (nine CRUK0733 were sacrificed).

3.2.7 Optimization of Genomic DNA Extraction and Quantification

Prior to this project, the genomic DNA (gDNA) extraction and quantification process was optimized for barcoding studies and included the extraction of gDNA from cells from start of the experiment (T0) and end of the screen (Tn) using the Wizard Genomic DNA Purification Kit (Promega). While this kit was scalable and offered an effective way to extract high quality gDNA from cultured cells and mouse brains, it was not specifically designed for extracting gDNA from mouse lungs. For the purposes of our *in vivo* screen, we needed a kit that not only allowed us to extract gDNA from the T0 cell pellet ($\sim 30 \times 10^7$ cells), but also from injected mouse lungs, lung tumors, and brains. The Gentra Puregene

Tissue Kit (Qiagen, #158689) offered a scalable protocol that we optimized for brain and lung tissue processing, and we were able to extract high yield gDNA for downstream purposes.

When quantifying the extracted gDNA, we made a comparison between NanoDrop UV spectrophotometry (routine technique for DNA concentration quantification used in Singh laboratory) and Qubit 2.0 Fluorometer using Qubit using double-stranded DNA (dsDNA) Broad Range Assay reagents (Thermo Fisher, Q32853) in assessing the concentration of gDNA extracted from mouse brains and lungs. We observed a difference between DNA concentration values measured by NanoDrop and Qubit **(Supplementary Figure 4)**. As discussed in Methods and Materials previously, this distinction may be due to the limited ability of NanoDrop UV spectrophotometry to distinguish DNA and RNA in samples that contain both, which is not a limitation of Qubit fluorometry. This experiment illustrated differences in quantifying gDNA with NanoDrop *vs* Qubit and pointed us to the direction of using Qubit as the standard method for acquiring accurate measurements of DNA concentration.

3.3 Short-Term Next Steps

Currently, all mice involved in the CRUK0748 CRISPRa screen have reached endpoint (between days 25-29 post-injection), and all tissue has been extracted, imaged, and frozen for gDNA extraction. However, out of the mice involved in the CRUK0733 CRISPRa screen, nine mice have reached endpoint and 20 mice are currently alive. Our next immediate step is to submit T0 samples from both screens for sequencing to evaluate the quality and representation of the CRISPRa-transduced cell population injected into the

mouse lungs. We will next evaluate whether mice involved in the CRUK0733 screen display any brain metastases (through testing a batch of mouse brains for the presence of human tumor cells *via* flow cytometric analysis and RT-PCR analysis on GFP and human housekeeping gene markers). If mice show unsubstantial brain metastases, we will consider this screen replicate unusable for mouse brain sequencing purposes, while still harvesting all tissues for further analyses in the future.

Upon extraction of tissues that will be analyzed *via* NGS, primary lung tumors, BM, and other solid organ metastases will be snap-frozen using liquid nitrogen, and gDNA will isolated from brains, lungs, and lung tumors of the mice at a later time. Genomic DNA will be extracted from individual tissue samples (individual brain, lungs/lung tumors from each mouse) and sequenced separately. Sequencing library preparation and NGS will be done at Donnelly Sequencing Centre using an Illumina sequencer, and sgRNA abundance determined using published algorithms (Sanson et al., 2018).

Furthermore, the Singh laboratory has produced an RNA sequencing dataset from lung-to-brain metastasis initiating cells identifying a list of genes that are upregulated to promote the formation of premetastatic brain lesions, which we can cross-reference to validate our screen hits (Singh et al., 2018).

a

Plate 200uL of cell mixture on each 150 mm agar plate containing ampicillin

Scrape colonies using LB broth containing ampicillin and pool colonies from all plates

Weigh the wet pellet and isolate DNA accordingly

x40

14-16 hours at 30°C

Incubate while stirring at room temperature for 1 hour. Centrifuge at 4°C for 10 min

Four electroporation reactions using 25uL of Endura© cells and 2uL of the library (50ng/uL) per reaction

Pool electroporated cells and incubate at 37°C while shaking for 1 hour

Dilution plate of 40,000x diluted cell mixture to count colonies to verify transformation efficiency

Count colonies

To reach 500X library coverage (56,762 sgRNAs), we need 56,762 x 500 = **28,381,000 colonies** in total. When we dilute the Endura cell mixture 40,000 times, the number of required colonies for accurate representation is 28381000/40,000= **710 colonies**.

Therefore, by counting the colonies on the 40,000 dilution plate, we can estimate the efficiency of library transformation as a first line of quality control.

b

Next Generation Sequencing

50×10^6 (for 500X library)

2×10^6 NSCLC cells

Flow Cytometry

dCas9-LTX 731/ LTX 782 lung cancer cells expresssing GFP-luciferase

Lentiviral packaging and introduction of the ge-nome-wide CRISPRa library into cells

After 15-20 cell doublings, harvest cells containing sgRNAs and inject intratho-racically

Engraftment and Metastasis

Immunohistochemistry

Figure 7. Schematic of CRISPRa Library Preparation and In Vivo CRISPRa Screen Workflow. a) Workflow of CRISPRa library amplification and colony counting calculations on the 40,000 dilution plate. **b)** *In vivo* CRISPRa screen workflow for lung-to-brain metastasis.

A
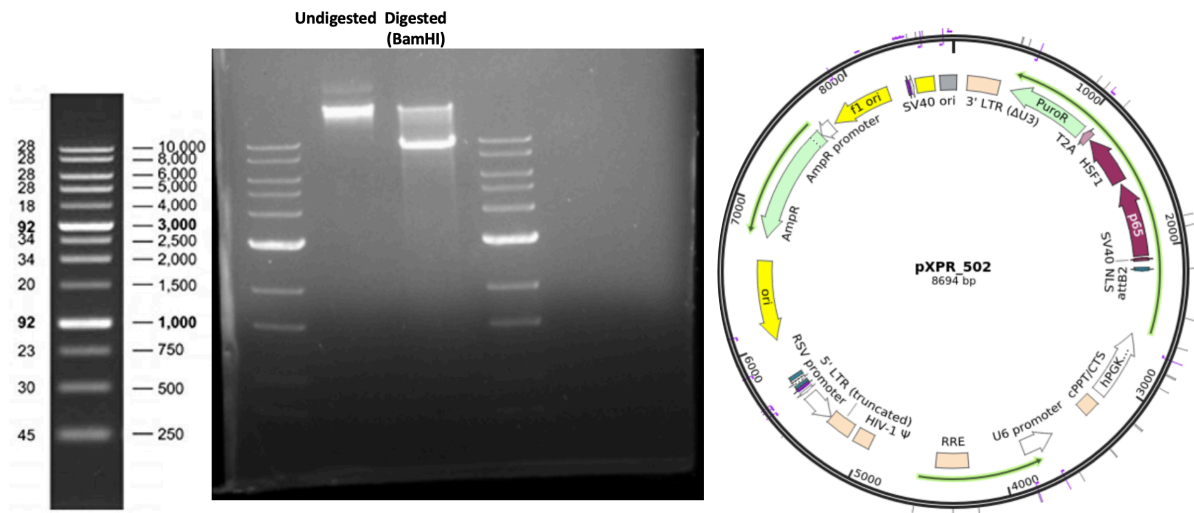
B
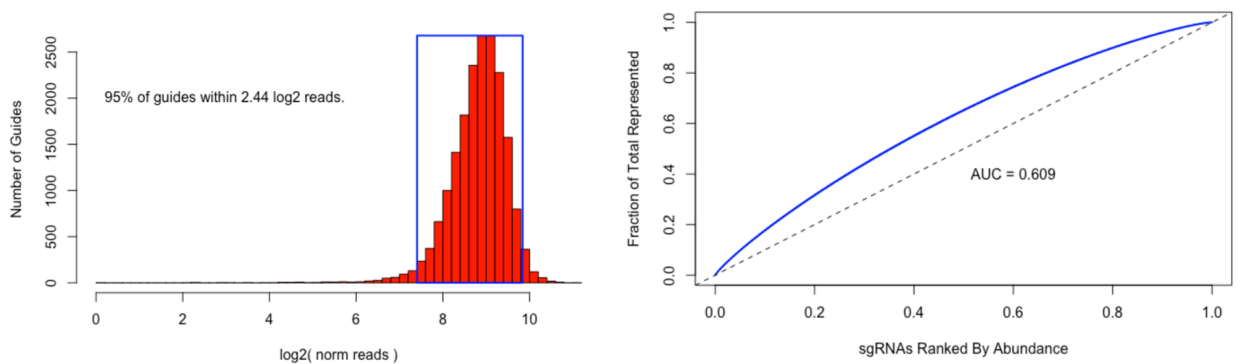
Figure 8. CRISPRa Library Quality Control. A) Library pool plasmid size was confirmed using restriction enzyme BamHI digest and DNA electrophoresis. **B)** Normalized read count distribution plot depicts a normal distribution, with 95% of guides found within a tight distribution. Area Under the Curve (AUC) plot demonstrates a value close to 0.5, indicating that the library has equal representation of all guides.
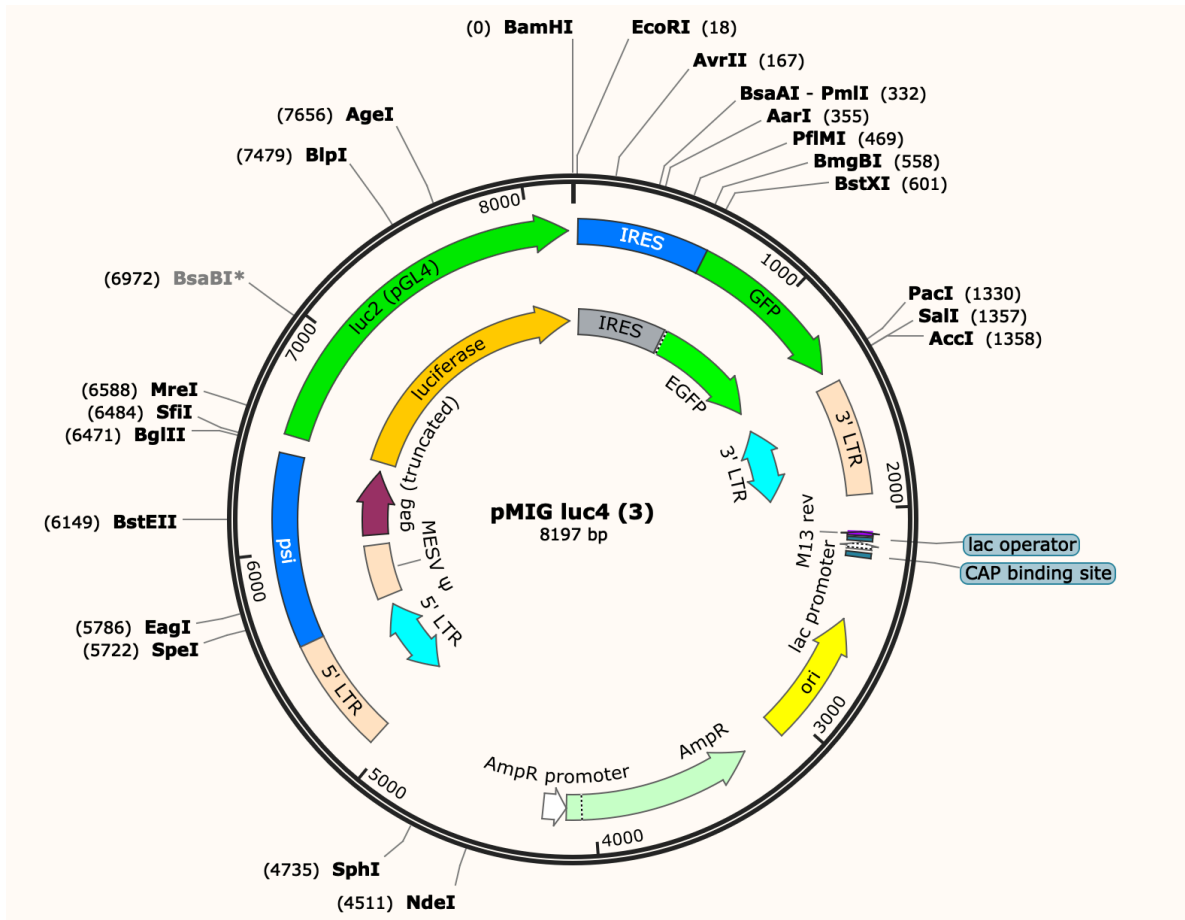
Supplementary Figure 2. Plasmid map of pMIG luc4 (3) (GFP-Luciferase construct)

	KRAS	TP53	EGFR	FGFR1	MET	NRAS	PDP1	PIK3CA	CDKN2A	ERBB2	MDM2	FREM2	STK11	PI4KA	VCAN	SUMF1	GRM1	FERMT1	ABCA13	IL12RB2
CRUK0748																				
CRUK0733																				

Likely clonal   Detected at low VAF, not in all regions, likely subclonal   Not detected, presumed WT
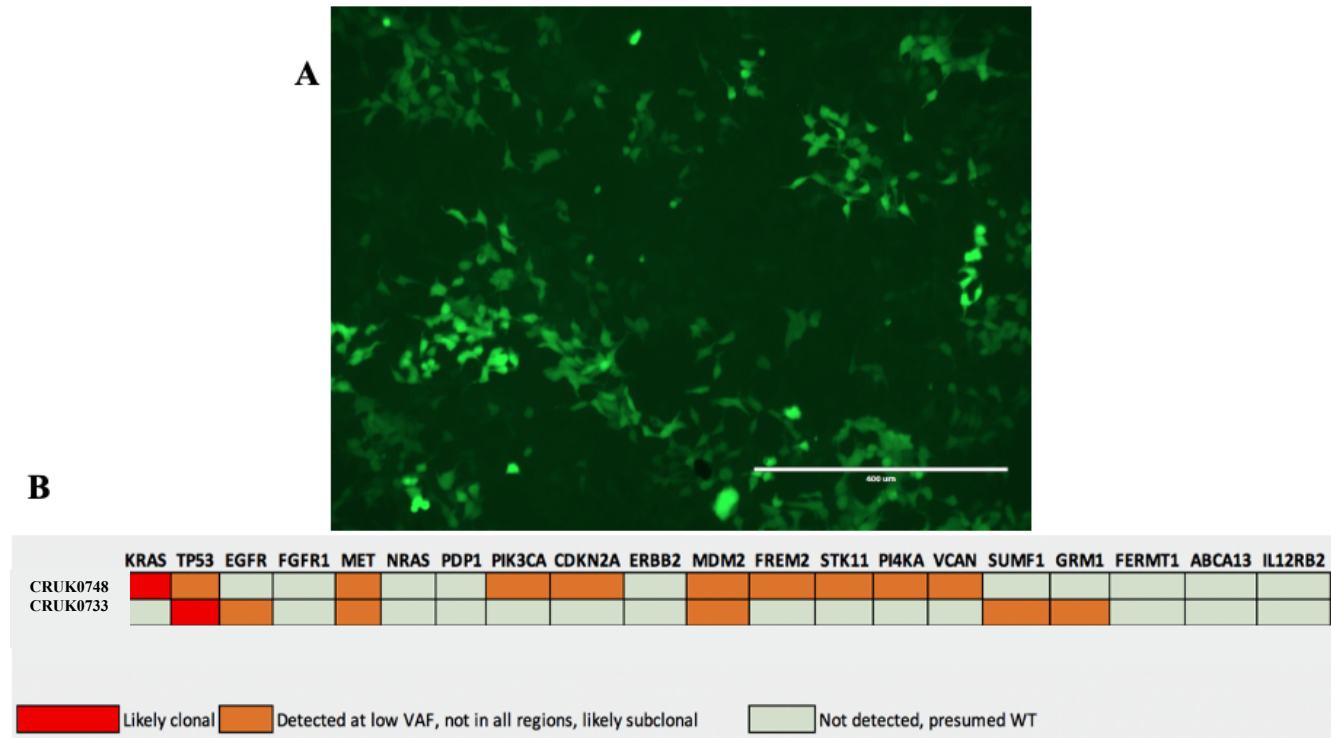
Supplementary Figure 3. Characterization of patient-derived CRUK0733 and CRUK0748 TRACERx NSCLC samples. A) Fluorescence microscopy shows GFP-(+) GFP-luc-CRUK0733 cells. **B)** Genetic mutational landscape of CRUK0733 and CRUK0748 determined through Whole Exome Sequencing.
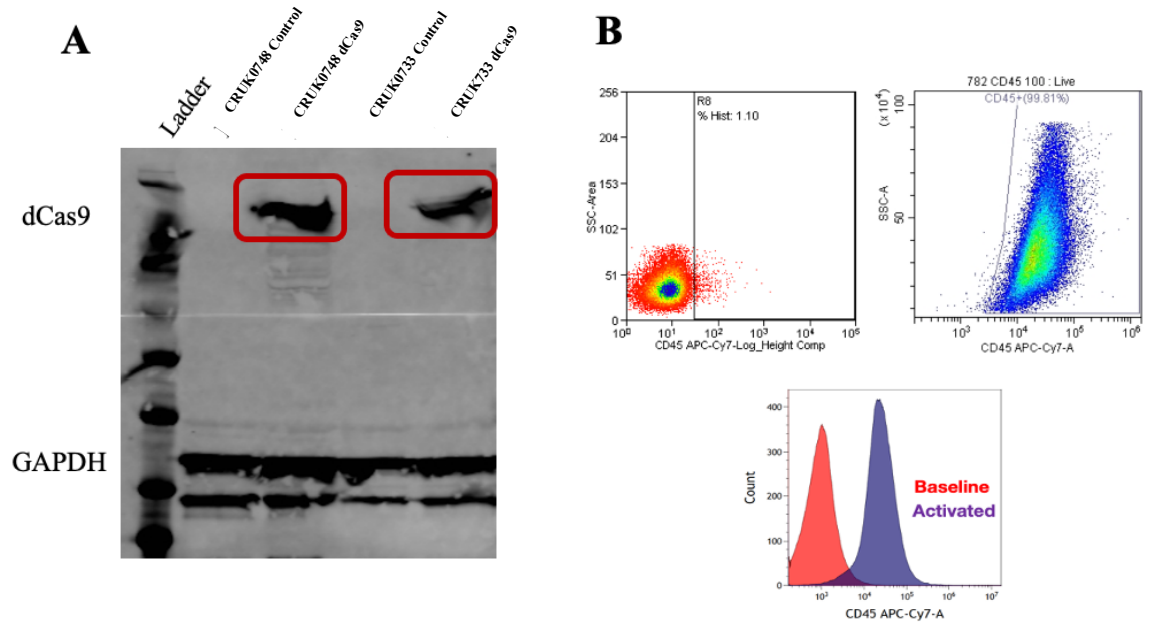
Figure 9. dCas9 Expression in dCas9-VP64-GFP-Luc CRUK0748 and CRUK0733 NSCLC cells. A) dCas9 protein expression following lentiviral transduction was confirmed in CRUK0748 and CRUK0733 cells through Western Blotting. Lanes from left to right: BLUeye Prestained Protein Ladder, CRUK0733 untransduced control, CRUK0748 transduced with dCas9 lentivirus, CRUK0733 untransduced control, CRUK0733 transduced with dCas9 lentivirus. dCas9 bands were visualized at a molecular weight of ~165kDa. GAPDH was used as loading control. **B)** Flow cytometric analyses between dCas9-VP64$^-$ CRUK0733 and dCas9-VP64$^+$ CRUK0733 cells transduced with sgCD45 lentivirus displays a 32-fold overexpression of CD45 in dCas9-VP64$^+$ CRUK0733 compared to baseline.
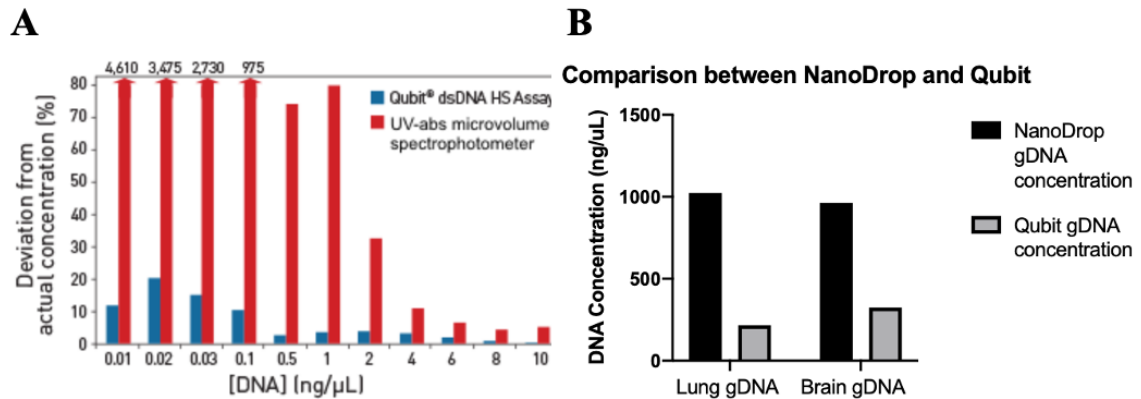
Supplementary Figure 4. Comparison between Ultraviolet (UV) Spectrophotometry and Fluorometry in Quantifying DNA Concentrations. A) Ten replicates of DNA samples at concentrations from 0.01 to 10 ng/µL were assayed using the Invitrogen Quant-iT DNA HS Assay on the Qubit Fluorometer according to the standard kit protocol. The same concentrations of DNA were measured in 10 replicates using a UV-absorbance microvolume spectrophotometer, and results were compared for accuracy (Thermo Fisher). **B)** Comparisons between gDNA concentration measured using NanoDrop and Qubit display differences in double-stranded DNA quantification.

A
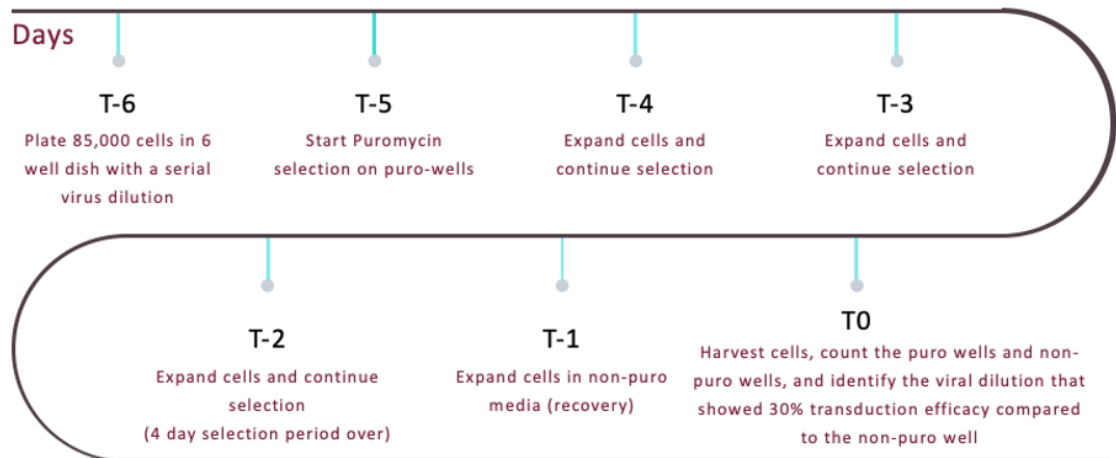
B
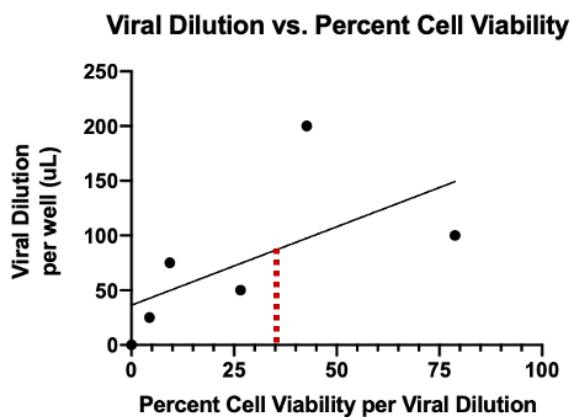
C
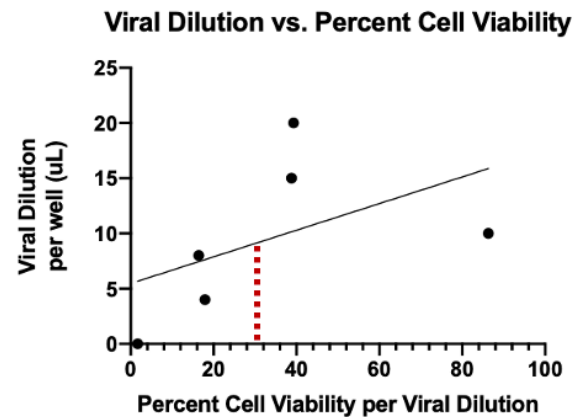
Supplementary Figure 5. Multiplicity of Infection (MOI) Experiments. A) Schematic of MOI experimental timeline. **B)** Linear regression of dataset displaying CRISPRa lentivirus viral dilution and corresponding percent CRUK0748 dCas9-VP64-GFP-Luc cell viability (ratio between puromycin-treated and puromycin-untreated wells receiving the same viral dilution). **C)** Linear regression of dataset displaying CRISPRa lentivirus viral dilution and corresponding percent CRUK0733 dCas9-VP64-GFP-Luc cell viability (ratio between puromycin-treated and puromycin-untreated wells receiving the same viral dilution). The dashed purple lines on both B and C graphs indicate 30% cell viability and the corresponding y-axis values indicate the viral dilutions to be used to reach an MOI of ~0.3 for each cell line.
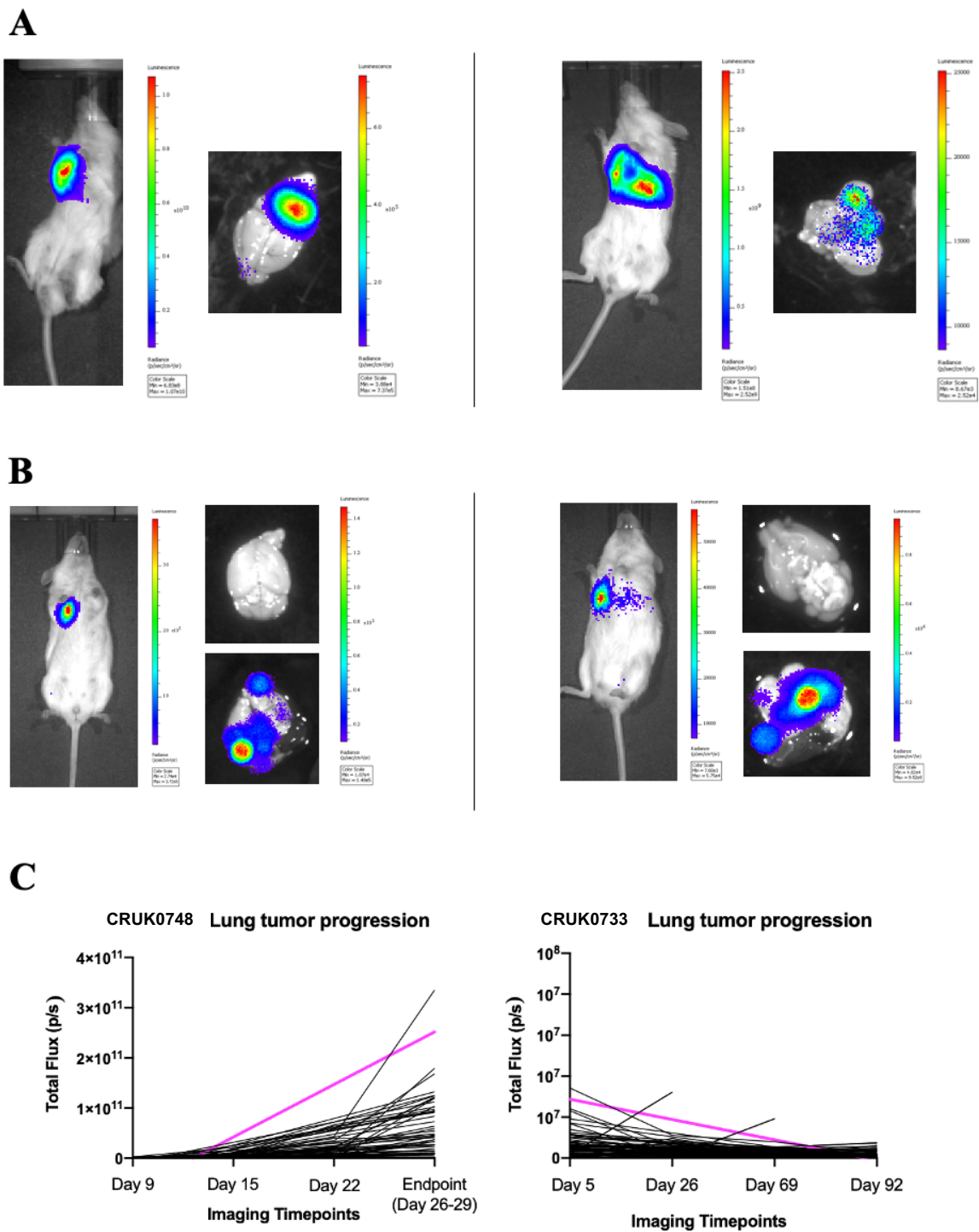
Figure 10. Comparison of CRUK0748 and CRUK0733 CRISPRa *in vivo* screens. A) Mice injected intrathoracically with CRISPRa-transduced and control CRUK0748 cells reached endpoint, and lung tumor signal as well as brain metastases were analyzed using

bioluminescent IVIS imaging *in vivo* and *ex vivo*. The right panel displays an CRUK0733 CRISPRa screen mouse with *in vivo* lung tumor bioluminescent signal, in addition to *ex vivo* images of brain and lung. The left panel shows an CRUK0748 control mouse with *in vivo* lung tumor bioluminescent signal, in addition to *ex vivo* images of brain and lung. **B)** Mice injected intrathoracically with CRISPRa-transduced and control CRUK0733 cells reached endpoint, and lung tumor signal as well as brain metastases were analyzed using bioluminescent IVIS imaging *in vivo* and *ex vivo*. The right panel displays an CRUK0733 CRISPRa screen mouse with *in vivo* lung tumor bioluminescent signal, in addition to *ex vivo* images of brain and lung. The left panel shows an CRUK0733 control mouse with *in vivo* lung tumor bioluminescent signal, in addition to *ex vivo* images of brain and lung. **C)** Lung tumor growth progression for all mice in CRUK0748 (right) and CRUK0733 (left) CRISPRa screen was plotted. The purple linear regression lines display the trend in lung tumor growth for each screen.

CONCLUSION AND FUTURE DIRECTIONS

4.1 Discussion

Brain metastasis (BM) is the most common tumor of the central nervous system, presenting ten times more frequently than primary brain tumors in the clinic (Palmieri, 2012). As systemic therapies for primary cancers improve, circulating tumor cells are allowed more time to metastasize and seed other organs. Twenty to forty percent of people with cancer will develop secondary brain metastasis (BM), the majority of cases originating from the lung (20-56% of patients), breast (5-20%), and melanoma (7-16%), with increasing incidence as cancer patients continue to live longer due to improved treatments for their primary disease (Achrol et al., 2019).

Lung cancer is the most commonly diagnosed cancer and the leading cause of cancer deaths in both men and women in Canada. It is estimated that in 2019 alone, 29,300 Canadians were diagnosed with lung cancer, representing 13% of all new cancer diagnoses in 2019. On average, 80 Canadians will be diagnosed with lung cancer every day and 58 Canadians will die from lung cancer every day. Unfortunately, the median survival for patients with BM is only 2-3 months without treatment and 4-12 months with treatment (Ba, Jandial, Nesbit, Badie, & Chen, 2015), with dismal overall 2-year and 5-year survival rates between 8.1% and 2.4%, respectively (Hall, Djalilian, Nussbaum, & Cho, 2000), reflecting a large unmet need for identifying novel therapeutic targets for preventing BM.

Genetic profiling of patient lung adenocarcinoma has identified that driver mutations in *EGFR* and the presence of *ALK* gene rearrangement increases the prevalence of the formation of BM (Collisson et al., 2014; Hayes et al., 2006). A landmark study by

Brastianos and colleagues tracked the genetic evolution of 86 matched primary and BM patient tumor samples (the majority of samples comprised of lung, breast, and renal cell carcinoma) and identified both common and divergent genetic signatures between matched primary and metastatic tissues, suggesting the ability of BM to undergo branched evolution (Brastianos et al., 2015). These signatures included gene amplifications in *MCL1*, *CCNE1*, *ERBB2*, *EGFR*, *MYC*, *MET*, *CDK6*, and *AKT2* in the BM of lung, breast, and melanoma cancer patients, underscoring the therapeutic potential of targeted small molecule inhibitors against some of these gene products to treat BM. However, this study more strikingly demonstrated that many metastatic brain tumors had distinct gene signatures compared to that of their matched primary samples, suggesting that systemic therapies targeted at primary tumors alone may not be suitable for the treatment of their corresponding BM. These results serve to underscore the need for continued efforts in discovering drivers of BM as a means to offer novel targeted therapies to these patients.

Several preclinical small animal models of lung cancer have been developed to recapitulate the etiopathogenesis of lung cancer formation, invasion, and metastasis. These models allow for investigators to study the mechanisms of lung cancer progression and also serve as *in vivo* platforms for therapeutic discovery. Functional genomics employs perturbations in gene function to address biological questions (Hartenian & Doench, 2015). This tool has proven to be extremely powerful in helping elucidate disease processes and the identification of novel targeted therapies in medicine. One effective and powerful way of studying this is using the CRISPR/Cas9 gene editing platform to perform genome-wide

perturbation studies in primary lung cancer cells using LBM models to determine how changes in gene function affect LBM process (Singh, Venugopal, et al., 2017).

In comparison to previous literature, our platform has the added ability to investigate the metastasis of lung tumors engrafting in an orthotopic location, as well as utilize patient-derived samples to potentially uncover clinically relevant biology in a gain-of-function genomic screen. To our knowledge, this study is the first CRISPR activation screen in an orthotopic mouse model of lung-to-brain metastasis that utilizes patient-derived NSCLC cells.

4.1.1 Development of an Orthotopic PDX Mouse Model of Lung-to-Brain Metastasis

In Chapter 2, we discuss the development of a PDX murine model of NSCLC-BM that recapitulates the brain metastatic cascade and is suitable for conducting a functional genomics study. Patient-derived xenograft (PDX) models that involve the injection of human lung cancer cells orthotopically into the lungs of immunocompromised mice allow for implantation of a variety of cell lines, both immortalized or derived from primary tumors surgically removed from patients (primary patient-derived cell lines), allowing for their use in personalized medicine applications that therefore bear more clinical relevance (Dong et al., 2010; Fichtner et al., 2008; Merk, Rolff, Becker, Leschber, & Fichtner, 2009). Prior to this thesis, an LBM mouse model created within the Singh laboratory was utilized to model LBM pre-clinically. While this model was functional for small scale genomic or drug screens, it did not accommodate cell numbers larger than 5×10^5 cells and did not use a direct injection route into the lung parenchyma as it was not surgically invasive. The ideal LBM model for this project needed to allow for implantation of tumor cells directly into

the lung parenchyma under the least invasive and painful conditions allowing for minimal procedural morbidity and mortality with highest success at inducing a focal tumor in the lungs of mice and higher number of cells ($2\text{-}5\text{x}10^6$ cells).

Stable expression of reporter proteins such as firefly luciferase in the cells prior to implantation further allows for tumor tracking *in vivo* using bioluminescent IVIS imaging for monitoring of tumor growth, metastasis, and response to therapies (Nogawa et al., 2005). In particular, IVIS is highly sensitive for detecting tumor cells in the brain, with the ability to detect bioluminescence from as few as 1500 to 3000 engrafted cells in the brain through intact skull, connective tissue, and skin of mice (Aswendt, Adamczak, Couillard-Despres, & Hoehn, 2013).

Our PDX model of NSCLC-BM accurately recapitulated the brain metastatic propensity of pro-metastatic and non-metastatic patient-derived cell lines *in vivo*. One limitation in this model is the number of cells that can successfully enter, engraft, and grow in the limited space of one lung lobe through intrathoracic injections. Other groups have devised animal models that implant cells through the trachea, which may circumvent the issue of limited space in the lung parenchyma by directly entering lung tissue (Nakajima et al., 2014). However, large injection volumes and cell densities have not been explored in this intratracheal model of inducing lung tumors and may be a valuable avenue to investigate in the future.

4.1.2 Identification of Genetic Drivers of LBM via *a Genome-Wide* in vivo *CRISPR Activation Screen*

In Chapter 3, we discuss the *in vivo* utilization of the gain-of-function genomics screening platform, CRISPRa, in our model of NSCLC-BM. The traditional use of CRISPR/Cas9 gene editing to achieve gene knockout at a genome-wide scale has allowed for broad screening of genes that are essential to cell viability (Wang, Wei, Sabatini, & Lander, 2014). This has been particularly useful in identifying vulnerabilities in cancer cells that drive oncogenesis (Shalem et al., 2014). However, the nature of these *negative* selection screens is such that they are limited to the extent that the perturbation is present in the system and as such the significance in discerning the loss of a specific gene function to impart a particular phenotype often requires a secondary screen to further validate the results of the initial screen (Hartenian & Doench, 2015).

Recent refinement of the CRISPR-Cas9 system to achieve either gene *i*nhibition (CRISPR*i*) or *a*ctivation (CRISPR*a*) has allowed investigators to systematically study whole genome-wide perturbations in cells in a tunable, orthogonal, and multiplexed fashion with widespread applications throughout the fields of biology and medicine (Gilbert et al., 2014; Joung et al., 2017; Kampmann, 2018; Konermann et al., 2015; Martella et al., 2019; Sanson et al., 2018). In particular, recent advances in performing genome-wide functional genomics screening in murine models have allowed scientists to study mechanisms of lung cancer oncogenesis (Sanchez-Rivera et al., 2014) and metastasis (S. Chen et al., 2015), increasing the probability of discovering novel targets with therapeutic implications. While loss of function studies such as creating insertions/deletions (indels) in the genetic sequence

are the hallmark of forward genetics, published studies have defined essentiality as growth and survival of cells, which cannot fully capture the intricacies of the metastatic cascade including the steps of invasion or migration. Instead, other genetic modulations enabled using the CRISPR system, for instance transcriptional activation, could potentially better interrogate the processes underlying cancer metastasis.

CRISPRa is an umbrella term representing systems involving a non-catalytic, dead Cas9 (dCas9) protein, alongside a transcriptional activation complex. To study the effects of gene activation on LBM formation, we performed an *in vivo* genome-wide CRISPRa screen using our established GFP-Luc CRUK0733 (non-metastatic) and CRUK0748 (metastatic) PDX NSCLC-BM mouse models. We transduced the whole-genome CRISPRa library into dCas9-VP64-GFP-Luc CRUK cells at a low MOI of ~0.3 at a representation of at least 500 cells per sgRNA (500X representation) taking into account ~ 30-50% transduction efficiency (Brown, Mair, Soste, & Moffat, 2019).

CRISPR activation was chosen as the method to interrogate the genetic underpinnings of LBM because of the unique insight it can provide into genetic drivers as opposed to essential genes for proliferation/metastasis. Gain-of-function screens have superior signal-to-noise characteristics because it is generally easier to see a positive signal against a background of negatives than the other way around (Kaelin, 2017). Positive selection screens are less likely than negative selection screens to produce signals that have relatively trivial or uninteresting explanations. This is because there are more trivial ways to make a complex biological process perform worse than there are ways to make it perform better (Kaelin, 2017).

Conducting the CRISPRa screen using the Calabrese library at 500X coverage required a post-transduction NSCLC cell population of $\sim30\times10^6$ cells to be injected into mice. Upon assessing lung tumor engraftment rates, we realized that it was not feasible to inject the entire NSCLC cell population into one mouse lung. Therefore, we chose the approximate number of cells that was shown to have engrafted into the lung parenchyma after one week, 2×10^6 cells, as the number of cells injected per mouse. We divided the total number of 50×10^6 cells that needed to be injected for one replicate of the CRISPRa screen (added 20×10^6 cells to the initial 30×10^6 to buffer for cell loss during injection and cell death prior to injection) by 2×10^6 to calculate the number of mice required for each replicate, which resulted in 25 mice injected with NSCLC-CRISPRa tumor cells.

Lung tumor growth rates in CRUK0748 and CRUK0733 screens followed different trajectories **(Figure 10C)**. Illustrated through IVIS imaging, CRUK0748 mice followed a strong upward trend compared to CRUK0733 mice, which showed a plateaued lung tumor signal. This difference in lung tumor development and subsequent formation of brain metastases **(Figure 10A-B)** may have been due to the underlying genetic differences between the pro-metastatic and non-metastatic NSCLC lines and can be explored as a future research question. Moreover, overexpression of genes through CRISPR activation may have had distinct influences on the tumorigenicity and metastatic properties of CRUK0748 and CRUK0733, due to underlying genetic differences. We also hypothesize that the lack of brain metastases in CRUK0733 brains that were tested so far could be due to the possibility that overexpression of one gene per cell may not have been effective in activating tumor development or metastasis in this cell line. Future studies may investigate

multiplexed endogenous gene activation (Cheng et al., 2013) in the context of brain metastasis to uncover **s**ynergistic tendencies between different cellular pathways that can potentially promote brain metastasis.

4.2. Future Directions

We have developed a patient-derived xenograft (PDX) mouse model of LBM by direct injection of genetically annotated patient-derived non-small cell lung cancer (NSCLC) cell lines **(Figure 4)** into the lungs of immune-compromised SCID mice and have tracked their metastasis to the brain using IVIS following stable expression of firefly luciferase. We have also conducted two CRISPR activation screens in two NSCLC lines, non-metastatic and pro-metastatic, using our murine model. Future directions for this project focus on sequencing mouse tissue gDNA, deriving candidate driver gene hits, validation of hits *in vitro* and *in vivo*, and confirming the clinical relevance of hits through analysis of patient-derived matched lung tumor and brain metastasis samples.

4.2.1. Sequencing Mouse Tissue and Deriving Clinically Relevant Candidate Genes

Short-term future directions include extraction of high quality gDNA from harvested CRUK0748 mouse brains, lungs, and lung tumors, subsequent sgRNA inserts amplification, Next Generation Sequencing using an Illumina sequencer, and sgRNA abundance determination using published algorithms (Sanson et al., 2018).

Following completion of Illumina sequencing, 20-bp gRNA sequences are extracted from FASTQ files by trimming reads according to constant sequence anchors. Trimmed reads are aligned to a FASTA file of gRNA sequences from Calabrese CRISPRa library using Bowtie (v0.12.8) (Langmead, Trapnell, Pop, & Salzberg, 2009). Processed reads are

tallied for each sample and merged into a matrix. To begin quantifying the normalized read counts of guides in each screen, log2 fold change (LFC) of each gRNA are quantified by comparing read-depth-normalized gRNA counts at the beginning of each screen (T0) to the end of each screen (Tn). T0 signifies the cell population that was directly injected into mouse lungs. To perform quality control analysis, the LFC for all gRNAs targeting a single gene will be averaged, with three gRNAs targeting each gene in the library.

4.2.2 Validation of Hits through in vitro *and* in vivo *Experiments*

From the identified target list from CRISPRa analyses, we will use stringent criteria in our *in silico* assessment that include target novelty, differential gene expression relative to normal tissues (using a publicly available TCGA database, GlioVis), and association with clinically-relevant measures such as expression levels and patient survival in lung cancer patients from publicly available databases to further narrow down the list. The top ten highest ranked guides isolated from BM will be validated in at least three additional annotated CRUK lines *in vitro*, and the top three hits from *in vitro* studies will be validated *in vivo*. We already have access to these lines both from Swanton lab as well as Shargall lab.

The top ten hits from the screen will be functionally validated *in vitro* by transducing non-metastatic CRUK cells (n=5) with CRISPRa vectors with target sgRNA or control vector, and evaluating changes in proliferation and migration through our optimized protocols (Singh, Venugopal, et al., 2017).

In vivo validation will be performed on the top three hits from *in vitro* studies. We will use NSCLC lines (including CRUK lines) that are transduced with CRISPRa vectors

selectively targeting top gene hits. We will test the efficacy of three designed sgRNA constructs per gene *in vitro* and choose the best guide to be used in animal studies. The transduced NSCLC cells will be xenografted into lungs of NSG mice to assess the effects of activation of key putative drivers of BM by evaluating the prevalence of BM and survival. We will also account for sex differences by obtaining equal numbers of male and female CRUK lines and validate our hits in male and female SCID mice, respectively.

4.2.3. Immunohistochemical Validation of Drivers of Lung-to-Brain metastasis in Matched Patient Primary Lung Tumors and Brain Metastases

Through our collaboration with Dr. Yaron Shargall, we can access a bank of patient lung tumor and matched brain metastasis paraffin-embedded tissue blocks. We can utilize this valuable resource to create a Tissue Microarray (TMA) of patient-derived matched lung tumor and brain metastasis samples that can be sectioned multiple times and is suitable for the study of a large cohort of patient samples at the same time.

To validate the clinical relevance of proteins that are overexpressed upon CRISPR activation and subsequently enriched in the BM of the NSCLC PDX mice, we will perform immunohistochemistry comparing differential expression of the top three short-listed and validated hits from our screen using the TMA of matched primary NSCLC patient tissues with their corresponding BM. This will more importantly demonstrate where in the metastatic cascade these genes are upregulated, whether it be in the initial stages of epithelial-to-mesenchymal transition to allow for hematogenous escape of primary lung tumors cells, or the mesenchymal-to-epithelial transition which allows for intravasation from the circulation into brain niche, and/or the processes involved in the seeding of the

brain to form a premetastatic lesion which will then go on to form a mature metastasis. We hope that gaining an understanding into genetic drivers of lung tumor development and brain metastasis will facilitate a more targeted approach towards drug discovery and will ultimately improve the lives of patients who grapple with NSCLC-BM.

REFERENCES

Achrol, A. S., Rennert, R. C., Anders, C., Soffietti, R., Ahluwalia, M. S., Nayak, L., … Chang, S. D. (2019). Brain metastases. *Nature Reviews Disease Primers*, *5*(1). https://doi.org/10.1038/s41572-018-0055-y

Aswendt, M., Adamczak, J., Couillard-Despres, S., & Hoehn, M. (2013). Boosting Bioluminescence Neuroimaging: An Optimized Protocol for Brain Studies. *PLoS ONE*. https://doi.org/10.1371/journal.pone.0055662

Ba, J. L. i., Jandial, R., Nesbit, A., Badie, B., & Chen, M. (2015). Current and emerging treatments for brain metastases. *Oncology (Williston Park, N.Y.)*.

Barker, F. G. (2004). Craniotomy for the Resection of Metastatic Brain Tumors in the U.S., 1988-2000: Decreasing Mortality and the Effect of Provider Caseload. *Cancer*, *100*(5), 999–1007. https://doi.org/10.1002/cncr.20058

Barnholtz-Sloan, J. S., Sloan, A. E., Davis, F. G., Vigneau, F. D., Lai, P., & Sawaya, R. E. (2004). Incidence proportions of brain metastases in patients diagnosed (1973 to 2001) in the Metropolitan Detroit Cancer Surveillance System. *Journal of Clinical Oncology*, *22*(14), 2865–2872. https://doi.org/10.1200/JCO.2004.12.149

Berghoff, A. S., & Preusser, M. (2015). The inflammatory microenvironment in brain metastases: Potential treatment target? *Chinese Clinical Oncology*. AME Publishing Company. https://doi.org/10.3978/j.issn.2304-3865.2015.06.03

Berghoff, A. S., Schur, S., Füreder, L. M., Gatterbauer, B., Dieckmann, K., Widhalm, G., … Preusser, M. (2016). Descriptive statistical analysis of a real life cohort of 2419 patients with brain metastases of solid cancers. *ESMO Open*, *1*(2). https://doi.org/10.1136/esmoopen-2015-000024

Brastianos, P. K., Carter, S. L., Santagata, S., Cahill, D. P., Taylor-Weiner, A., Jones, R. T., … Hahn, W. C. (2015). Genomic Characterization of Brain Metastases Reveals Branched Evolution and Potential Therapeutic Targets Genetic Divergence of Brain Metastases and Primary Tumors. https://doi.org/10.1158/2159-8290.CD-15-0369

Brauna, C. J., Brunoa, P. M., Horlbeckc, M. A., Gilbertc, L. A., Weissmanc, J. S., & Hemanna, M. T. (2016). Versatile in vivo regulation of tumor phenotypes by dCas9-mediated transcriptional perturbation. *Proceedings of the National Academy of Sciences of the United States of America*, *113*(27), E3892–E3900. https://doi.org/10.1073/pnas.1600582113

Brown, K. R., Mair, B., Soste, M., & Moffat, J. (2019). CRISPR screens are feasible in TP 53 wild-type cells . *Molecular Systems Biology*. https://doi.org/10.15252/msb.20188679

Cabezas, R., Ávila, M., Gonzalez, J., El-Bachá, R. S., Báez, E., García-Segura, L. M., … Barreto, G. E. (2014, August 4). Astrocytic modulation of blood brain barrier: Perspectives on Parkinson's disease. *Frontiers in Cellular Neuroscience*. Frontiers Research Foundation. https://doi.org/10.3389/fncel.2014.00211

Chavez, A., Scheiman, J., Vora, S., Pruitt, B. W., Tuttle, M., P R Iyer, E., … Church, G. M. (2015). Highly efficient Cas9-mediated transcriptional programming. *Nature Methods*, *12*(4), 326–328. https://doi.org/10.1038/nmeth.3312

Chen, G., Liu, X. yan, Wang, Z., & Liu, F. ying. (2010). Vascular endothelial growth factor C: the predicator of early recurrence in patients with N2 non-small-cell lung cancer. *European Journal of Cardio-Thoracic Surgery*, *37*(3), 546–551. https://doi.org/10.1016/j.ejcts.2009.08.005

Chen, G., Wang, Z., Liu, X. Y., & Liu, F. Y. (2011). High-level CXCR4 expression correlates with brain-specific metastasis of non-small cell lung cancer. *World Journal of Surgery*, *35*(1), 56–61. https://doi.org/10.1007/s00268-010-0784-x

Chen, S., Sanjana, N. E., Zheng, K., Shalem, O., Lee, K., Shi, X., … Sharp, P. A. (2015). Genome-wide CRISPR screen in a mouse model of tumor growth and metastasis. *Cell*, *160*(6), 1246–1260. https://doi.org/10.1016/j.cell.2015.02.038

Cheng, A. W., Wang, H., Yang, H., Shi, L., Katz, Y., Theunissen, T. W., … Jaenisch, R. (2013). Multiplexed activation of endogenous genes by CRISPR-on, an RNA-guided transcriptional activator system. *Cell Research*. https://doi.org/10.1038/cr.2013.122

Collisson, E. A., Campbell, J. D., Brooks, A. N., Berger, A. H., Lee, W., Chmielecki, J., … Cheney, R. (2014). Comprehensive molecular profiling of lung adenocarcinoma: The cancer genome atlas research network. *Nature*. https://doi.org/10.1038/nature13385

Dong, X., Guan, J., English, J. C., Flint, J., Yee, J., Evans, K., … Wang, Y. (2010). Patient-derived first generation xenografts of non-small cell lung cancers: Promising tools for predicting drug responses for personalized chemotherapy. *Clinical Cancer Research*. https://doi.org/10.1158/1078-0432.CCR-09-2878

Ebright, R. Y., Lee, S., Wittner, B. S., Niederhoffer, K. L., Nicholson, B. T., Bardia, A., … Micalizzi, D. S. (2020). Deregulation of ribosomal protein expression and translation promotes breast cancer metastasis. *Science*, *367*(6485), 1468–1473. https://doi.org/10.1126/science.aay0939

Fichtner, I., Rolff, J., Soong, R., Hoffmann, J., Hammer, S., Sommer, A., … Merk, J. (2008). Establishment of patient-derived non-small cell lung cancer xenografts as models for the identification of predictive biomarkers. *Clinical Cancer Research*. https://doi.org/10.1158/1078-0432.CCR-08-0138

Francia, G., Cruz-Munoz, W., Man, S., Xu, P., & Kerbel, R. S. (2011). Mouse models of advanced spontaneous metastasis for experimental therapeutics. *Nature Reviews Cancer*. https://doi.org/10.1038/nrc3001

Fushiki, H., Kanoh-Azuma, T., Katoh, M., Kawabata, K., Jiang, J., Tsuchiya, N., … Hayakawa, Y. (2009). Quantification of mouse pulmonary cancer models by microcomputed tomography imaging. *Cancer Science*, *100*(8), 1544–1549. https://doi.org/10.1111/j.1349-7006.2009.01199.x

Gavrilovic, I. T., & Posner, J. B. (2005, October). Brain metastases: Epidemiology and pathophysiology. *Journal of Neuro-Oncology*. https://doi.org/10.1007/s11060-004-

8093-6

Gilbert, L. A., Horlbeck, M. A., Adamson, B., Villalta, J. E., Chen, Y., Whitehead, E. H., … Weissman, J. S. (2014). Genome-Scale CRISPR-Mediated Control of Gene Repression and Activation. *Cell*. https://doi.org/10.1016/j.cell.2014.09.029

Gilbert, L. A., Larson, M. H., Morsut, L., Liu, Z., Brar, G. A., Torres, S. E., … Qi, L. S. (2013). XCRISPR-mediated modular RNA-guided regulation of transcription in eukaryotes. *Cell*, *154*(2), 442. https://doi.org/10.1016/j.cell.2013.06.044

Grzeskowiak, C. L., Kundu, S. T., Mo, X., Ivanov, A. A., Zagorodna, O., Lu, H., … Scott, K. L. (2018). In vivo screening identifies GATAD2B as a metastasis driver in KRAS-driven lung cancer. *Nature Communications*, *9*(1). https://doi.org/10.1038/s41467-018-04572-3

Hall, W. A., Djalilian, H. R., Nussbaum, E. S., & Cho, K. H. (2000). Long-term survival with metastatic cancer to the brain. *Medical Oncology*. https://doi.org/10.1007/BF02782192

Hartenian, E., & Doench, J. G. (2015). Genetic screens and functional genomics using CRISPR/Cas9 technology. *FEBS Journal*. https://doi.org/10.1111/febs.13248

Hayes, D. N., Monti, S., Parmigiani, G., Gilks, C. B., Naoki, K., Bhattacharjee, A., … Meyerson, M. (2006). Gene expression profiling reveals reproducible human lung adenocarcinoma subtypes in multiple independent patient cohorts. *Journal of Clinical Oncology*. https://doi.org/10.1200/JCO.2005.05.1748

Heyn, C., Ronald, J. A., Ramadan, S. S., Snir, J. A., Barry, A. M., MacKenzie, L. T., … Foster, P. J. (2006). In vivo MRI of cancer cell fate at the single-cell level in a mouse model of breast cancer metastasis to the brain. *Magnetic Resonance in Medicine*, *56*(5), 1001–1010. https://doi.org/10.1002/mrm.21029

Hsu, F., De Caluwe, A., Anderson, D., Nichol, A., Toriumi, T., & Ho, C. (2016). EGFR mutation status on brain metastases from non-small cell lung cancer. *Lung Cancer*, *96*, 101–107. https://doi.org/10.1016/j.lungcan.2016.04.004

Ito, R., Takahashi, T., Katano, I., & Ito, M. (2012, May). Current advances in humanized mouse models. *Cellular and Molecular Immunology*. https://doi.org/10.1038/cmi.2012.2

Jamal-Hanjani, M., Wilson, G. A., McGranahan, N., Birkbak, N. J., Watkins, T. B. K., Veeriah, S., … Swanton, C. (2017). Tracking the Evolution of Non–Small-Cell Lung Cancer. *New England Journal of Medicine*, *376*(22), 2109–2121. https://doi.org/10.1056/NEJMoa1616288

Jia, W., Martin, T. A., Zhang, G., & Jiang, W. G. (2013). Junctional adhesion molecules in cerebral endothelial tight junction and brain metastasis. *Anticancer Research*, *33*(6), 2353–2359. Retrieved from http://www.ncbi.nlm.nih.gov/pubmed/23749882

Jinek, M., Chylinski, K., Fonfara, I., Hauer, M., Doudna, J. A., & Charpentier, E. (2012). A programmable dual-RNA-guided DNA endonuclease in adaptive bacterial immunity. *Science*, *337*(6096), 816–821. https://doi.org/10.1126/science.1225829

Joung, J., Konermann, S., Gootenberg, J. S., Abudayyeh, O. O., Platt, R. J., Brigham, M. D., … Zhang, F. (2017). Genome-scale CRISPR-Cas9 knockout and transcriptional activation screening. *Nature Protocols*. https://doi.org/10.1038/nprot.2017.016

Kaelin, W. G. (2017). Common pitfalls in preclinical cancer target validation. *Nature Reviews Cancer*. https://doi.org/10.1038/nrc.2017.32

Kaminski, N., & Krupsky, M. (2004). Gene expression patterns, prognostic and diagnostic markers, and lung cancer biology. *Chest*, *125*(5 Suppl), 111S-5S. https://doi.org/10.1378/chest.125.5_suppl.111s-a

Kampmann, M. (2018). CRISPRi and CRISPRa Screens in Mammalian Cells for Precision Biology and Medicine. *ACS Chemical Biology*, *13*(2), 406–416. https://doi.org/10.1021/acschembio.7b00657

Konermann, S., Brigham, M. D., Trevino, A. E., Joung, J., Abudayyeh, O. O., Barcena, C., … Zhang, F. (2015). Genome-scale transcriptional activation by an engineered CRISPR-Cas9 complex. *Nature*. https://doi.org/10.1038/nature14136

Kwak, E. L., Bang, Y. J., Camidge, D. R., Shaw, A. T., Solomon, B., Maki, R. G., … Iafrate, A. J. (2010). Anaplastic lymphoma kinase inhibition in non-small-cell lung cancer.[Erratum appears in N Engl J Med. 2011 Feb 10;364(6):588]. *New England Journal of Medicine*, *363*(18), 1693–1703. https://doi.org/https://dx.doi.org/10.1056/NEJMoa1006448

La Russa, M. F., & Qi, L. S. (2015). The New State of the Art: Cas9 for Gene Activation and Repression. *Molecular and Cellular Biology*, *35*(22), 3800–3809. https://doi.org/10.1128/mcb.00512-15

Langmead, B., Trapnell, C., Pop, M., & Salzberg, S. L. (2009). Ultrafast and memory-efficient alignment of short DNA sequences to the human genome. *Genome Biology*. https://doi.org/10.1186/gb-2009-10-3-r25

Li, C., & Kasinski, A. L. (2020). In Vivo Cancer-Based Functional Genomics. *Trends in Cancer*. https://doi.org/10.1016/j.trecan.2020.07.004

Li, F., Huang, Q., Luster, T. A., Hu, H., Zhang, H., Ng, W. L., … Wong, K. K. (2020). In vivo epigenetic crispr screen identifies asf1a as an immunotherapeutic target in kras-mutant lung adenocarcinoma. *Cancer Discovery*, *10*(2), 270–287. https://doi.org/10.1158/2159-8290.CD-19-0780

Li, F., Ng, W.-L., Luster, T. A., Hu, H., Sviderskiy, V. O., Dowling, C. M., … Wong, K.-K. (2020). Epigenetic CRISPR Screens Identify Npm1 as a Therapeutic Vulnerability in Non–Small Cell Lung Cancer . *Cancer Research*, *80*(17), 3556–3567. https://doi.org/10.1158/0008-5472.can-19-3782

Li, W., Xu, H., Xiao, T., Cong, L., Love, M. I., Zhang, F., … Liu, X. (2014). MAGeCK enables robust identification of essential genes from genome-scale CRISPR/Cas9 knockout screens. *Genome Biology*, *15*(12), 554. https://doi.org/10.1186/preaccept-1316450832143458

Lim, F. (2002). RNA recognition site of PP7 coat protein. *Nucleic Acids Research*,

30(19), 4138–4144. https://doi.org/10.1093/nar/gkf552

Lin, X., & DeAngelis, L. M. (2015, October 20). Treatment of brain metastases. *Journal of Clinical Oncology*. American Society of Clinical Oncology. https://doi.org/10.1200/JCO.2015.60.9503

Luzzi, K. J., MacDonald, I. C., Schmidt, E. E., Kerkvliet, N., Morris, V. L., Chambers, A. F., & Groom, A. C. (1998). Multistep nature of metastatic inefficiency: Dormancy of solitary cells after successful extravasation and limited survival of early micrometastases. *American Journal of Pathology*, *153*(3), 865–873. https://doi.org/10.1016/S0002-9440(10)65628-3

Malladi, S., MacAlinao, D. G., Jin, X., He, L., Basnet, H., Zou, Y., … Massagué, J. (2016). Metastatic Latency and Immune Evasion through Autocrine Inhibition of WNT. *Cell*, *165*(1), 45–60. https://doi.org/10.1016/j.cell.2016.02.025

Manguso, R. T., Pope, H. W., Zimmer, M. D., Brown, F. D., Yates, K. B., Miller, B. C., … Haining, W. N. (2017). In vivo CRISPR screening identifies Ptpn2 as a cancer immunotherapy target. *Nature*, *547*(7664), 413–418. https://doi.org/10.1038/nature23270

Martella, A., Firth, M., Taylor, B. J. M., Göppert, A., Cuomo, E. M., Roth, R. G., … Fisher, D. I. (2019). Systematic Evaluation of CRISPRa and CRISPRi Modalities Enables Development of a Multiplexed, Orthogonal Gene Activation and Repression System. *ACS Synthetic Biology*. https://doi.org/10.1021/acssynbio.8b00527

Merk, J., Rolff, J., Becker, M., Leschber, G., & Fichtner, I. (2009). Patient-derived xenografts of non-small-cell lung cancer: a pre-clinical model to evaluate adjuvant chemotherapy? *European Journal of Cardio-Thoracic Surgery*. https://doi.org/10.1016/j.ejcts.2009.03.054

Mok, T. S., Wu, Y. L., Thongprasert, S., Yang, C. H., Chu, D. T., Saijo, N., … Fukuoka, M. (2009). Gefitinib or carboplatin-paclitaxel in pulmonary adenocarcinoma. *New England Journal of Medicine*, *361*(10), 947–957. https://doi.org/10.1056/NEJMoa0810699

Nakajima, T., Anayama, T., Matsuda, Y., Hwang, D. M., McVeigh, P. Z., Wilson, B. C., … Yasufuku, K. (2014). Orthotopic lung cancer murine model by nonoperative transbronchial approach. *Annals of Thoracic Surgery*, *97*(5), 1771–1775. https://doi.org/10.1016/j.athoracsur.2014.01.048

Nayak, L., Lee, E. Q., & Wen, P. Y. (2012). Epidemiology of brain metastases. *Current Oncology Reports*, *14*(1), 48–54. https://doi.org/10.1007/s11912-011-0203-y

Nogawa, M., Yuasa, T., Kimura, S., Kuroda, J., Sato, K., Segawa, H., … Maekawa, T. (2005). Monitoring luciferase-labeled cancer cell growth and metastasis in different in vivo models. *Cancer Letters*. https://doi.org/10.1016/j.canlet.2004.07.010

Palmieri, D. (2012). Central Nervous System Metastasis, the Biological Basis and Clinical Considerations, 237. https://doi.org/10.1007/978-94-007-5291-7

Patchell, R. A. (2003). The management of brain metastases. *Cancer Treatment Reviews*,

29(6), 533–540. https://doi.org/10.1016/S0305-7372(03)00105-1

Planchard, D., Popat, S., Kerr, K., Novello, S., Smit, E. F., Faivre-Finn, C., … Peters, S. (2018). Metastatic non-small cell lung cancer: ESMO Clinical Practice Guidelines for diagnosis, treatment and follow-up. *Annals of Oncology*, *29*, iv192–iv237. https://doi.org/10.1093/annonc/mdy275

Rosell, R., Carcereny, E., Gervais, R., Vergnenegre, A., Massuti, B., Felip, E., … Paz-Ares, L. (2012). Erlotinib versus standard chemotherapy as first-line treatment for European patients with advanced EGFR mutation-positive non-small-cell lung cancer (EURTAC): A multicentre, open-label, randomised phase 3 trial. *The Lancet Oncology*, *13*(3), 239–246. https://doi.org/10.1016/S1470-2045(11)70393-X

Sanchez-Rivera, F. J., Papagiannakopoulos, T., Romero, R., Tammela, T., Bauer, M. R., Bhutkar, A., … Jacks, T. (2014). Rapid modelling of cooperating genetic events in cancer through somatic genome editing. *Nature*. https://doi.org/10.1038/nature13906

Sanson, K. R., Hanna, R. E., Hegde, M., Donovan, K. F., Strand, C., Sullender, M. E., … Doench, J. G. (2018). Optimized libraries for CRISPR-Cas9 genetic screens with multiple modalities. *Nature Communications*, *9*(1). https://doi.org/10.1038/s41467-018-07901-8

Sequist, L. V., Yang, J. C. H., Yamamoto, N., O'Byrne, K., Hirsh, V., Mok, T., … Schuler, M. (2013). Phase III study of afatinib or cisplatin plus pemetrexed in patients with metastatic lung adenocarcinoma with EGFR mutations. *Journal of Clinical Oncology*, *31*(27), 3327–3334. https://doi.org/10.1200/JCO.2012.44.2806

Shalem, O., Sanjana, N. E., Hartenian, E., Shi, X., Scott, D. A., Heckl, D., … Doench, J. G. (2014). Shalem et al., 2014. *Science*, *343*(6166), 84–87. https://doi.org/10.1126/science.1247005.Genome-Scale

Shih, D. J. H., Nayyar, N., Bihun, I., Dagogo-Jack, I., Gill, C. M., Aquilanti, E., … Brastianos, P. K. (2020). Genomic characterization of human brain metastases identifies drivers of metastatic lung adenocarcinoma. *Nature Genetics*, *52*(4), 371–377. https://doi.org/10.1038/s41588-020-0592-7

Singh, M., Bakhshinyan, D., Venugopal, C., & Singh, S. K. (2017, September 19). Preclinical modeling and therapeutic avenues for cancer metastasis to the central nervous system. *Frontiers in Oncology*. Frontiers Media S.A. https://doi.org/10.3389/fonc.2017.00220

Singh, M., Venugopal, C., Tokar, T., Brown, K. R., McFarlane, N., Bakhshinyan, D., … Singh, S. K. (2017). RNAi screen identifies essential regulators of human brain metastasis-initiating cells. *Acta Neuropathologica*, *134*(6), 923–940. https://doi.org/10.1007/s00401-017-1757-z

Singh, M., Venugopal, C., Tokar, T., McFarlane, N., Subapanditha, M. K., Qazi, M., … Singh, S. K. (2018). Therapeutic targeting of the premetastatic stage in human lung-to-brain metastasis. *Cancer Research*. https://doi.org/10.1158/0008-5472.CAN-18-1022

Soda, M., Choi, Y. L., Enomoto, M., Takada, S., Yamashita, Y., Ishikawa, S., … Mano,

H. (2007). Identification of the transforming EML4-ALK fusion gene in non-small-cell lung cancer. *Nature*, *448*(7153), 561–566. https://doi.org/10.1038/nature05945

Sperduto, P. W., Chao, S. T., Sneed, P. K., Luo, X., Suh, J., Roberge, D., … Mehta, M. (2010). Diagnosis-Specific Prognostic Factors, Indexes, and Treatment Outcomes for Patients With Newly Diagnosed Brain Metastases: A Multi-Institutional Analysis of 4,259 Patients. *International Journal of Radiation Oncology Biology Physics*, *77*(3), 655–661. https://doi.org/10.1016/j.ijrobp.2009.08.025

Tanenbaum, M. E., Gilbert, L. A., Qi, L. S., Weissman, J. S., & Vale, R. D. (2014). A protein-tagging system for signal amplification in gene expression and fluorescence imaging. *Cell*, *159*(3), 635–646. https://doi.org/10.1016/j.cell.2014.09.039

TRAcking Cancer Evolution through therapy/Rx (TRACERx) clinical study | Crick. (n.d.). Retrieved February 5, 2020, from https://www.crick.ac.uk/research/labs/charles-swanton/areas-of-interest/tracking-cancer-evolution-through-therapy/rx-tracerx-clinical-study

Vanharanta, S., & Massagué, J. (2013, October 14). Origins of Metastatic Traits. *Cancer Cell*. https://doi.org/10.1016/j.ccr.2013.09.007

Villano, J. L., Durbin, E. B., Normandeau, C., Thakkar, J. P., Moirangthem, V., & Davis, F. G. (2015). Incidence of brain metastasis at initial presentation of lung cancer. *Neuro-Oncology*, *17*(1), 122–128. https://doi.org/10.1093/neuonc/nou099

Wang, T., Wei, J. J., Sabatini, D. M., & Lander, E. S. (2014). Genetic screens in human cells using the CRISPR-Cas9 system. *Science*. https://doi.org/10.1126/science.1246981

What is CRISPRa or CRISPR activation. (n.d.). Retrieved February 5, 2020, from https://horizondiscovery.com/en/resources/featured-articles/what-is-crispri-and-crispra

Wilmington, D. W. (2012). *Interpretation of nucleic acid 260/280 ratios*. *NanoDrop Products: T123 Technical Bulletin*.

Yoshimasu, T., Sakurai, T., Oura, S., Hirai, I., Tanino, H., Kokawa, Y., … Matsuura, N. (2004). Increased expression of integrin alpha3beta1 in highly brain metastatic subclone of a human non-small cell lung cancer cell line. *Cancer Science*, *95*(2), 142–148. https://doi.org/10.1111/j.1349-7006.2004.tb03195.x

APPENDIX: Academic Achievements

Manuscripts In Preparation and Under Review

1. Bassey-Archibong BI , Chokshi C , **Aghaei N**, Kieliszek A, Tatari N, McKenna D , Singh MS ,Subapanditha MK , Parmar A, Savage N, Lam F , Tokar T, Jurisica I, Provias J, Lu Y ,Venugopal C, Singh SK. (2021) Identification of an HLA-G/SPAG9/STAT3 axis presents a novel targetable liability in early brain metastases. *Manuscript in preparation*.

2. Chokshi CR, Tieu D, Brown KR, Venugopal C, Liu L, Kuhlmann L, Rossotti MA, Chan K, Tong A, Savage N, McKenna D, **Aghaei N,** Subapanditha M, Nachmani O, Ignatchenko V, Salamoun JM, Wipf P, Sharlow ER, Provias JP, Lu J-Q, Murty NK, Lazo JS, Kislinger T, Henry KA, Lu Y, Moffat J, Singh SK. (2021) Functional mapping reveals widespread remodelling at glioblastoma recurrence. *Manuscript under review.*

Scientific Meetings: Oral Presentations (*Presenter)

1. **Aghaei N*,** Lam FC, Venugopal C, Singh SK (2021). An *in vivo* functional genomics screen to identify novel drivers of lung-to-brain metastasis. Faculty of Health Sciences Graduate Plenary PechaKucha Oral Presentation Competition.

Scientific Meetings: Poster Presentations (*Presenter)

2. **Aghaei N*,** Lam FC, Venugopal C, Singh SK (2021). An *in vivo* functional genomics screen to identify novel drivers of lung-to-brain metastasis. Basic and Translational Omics of Brain Tumors and Their Microenvironment, Society of Neuro-Oncology.

3. **Aghaei N*,** Lam FC, Venugopal C, Singh SK (2021). In vivo functional genomic screen to identify novel drivers of lung-to-brain metastasis. Biochemistry and Biomedical Sciences Research Symposium.

4. **Aghaei N*,** Lam FC, Venugopal C, Singh SK (2021). An *in vivo* functional genomics screen to identify novel drivers of lung-to-brain metastasis. Ontario Institute for Cancer Research (OICR) Translational Research Conference.

5. Aghaei N*, **Lam FC, Venugopal C, Singh SK (2020).** Identificati**on of novel drivers of lung-to-brain metastasis through in vivo functional genomics. Society for Neuro-Oncology (SNO) Annual Scientific Meeting.**

6. Aghaei N*, **Lam FC, Venugopal C, Singh SK (2020).** Identificati**on of novel drivers of lung-to-brain metastasis through in vivo functional genomics. Society for Neuro-Oncology Annual Scientific Meeting.** Society of Neuro-Oncology **(SNO)** Brain Metastases Virtual Conference**.**

Scholarships & Awards
1. **Biochemistry and Biomedical Sciences Research Symposium** (Top Poster Prize)

McMaster University, 2021

2. **Faculty of Health Sciences Graduate Plenary** (PechaKucha Oral Presentation Competition Winner)
   McMaster University, 2021

3. **Ontario Graduate Scholarships (OGS)** ($15,000)
   McMaster University, 2020-2021

4. **Biochemistry Entrance Scholarship** ($1000)
   McMaster University, 2019

Scholarly Activities

1. *Catalyst* **(Biochemistry and Biomedical Undergraduate Journal) –** Journal Editor
McMaster University, 2020-2021

2. **Let's Talk Stem Cells** - Conference Content Developer
Let's Talk Science, 2021